12-9-2011

Body centric antennas for wireless cardiac monitoring

Travis Ann Nylin

BODY CENTRIC ANTENNAS FOR WIRELESS CARDIAC MONITORING

By

Travis Ann Nylin

A Thesis
Submitted to the Faculty of
Mississippi State University
in Partial Fulfillment of the Requirements
for the Degree of Master of Science
in Electrical Engineering
in the Department of Electrical and Computer Engineering

Mississippi State, Mississippi

December 2011

BODY CENTRIC ANTENNAS FOR WIRELESS CARDIAC MONITORING

By

Travis Ann Nylin

Approved:

Erdem Topsakal Associate Professor of Electrical and Computer Engineering (Major Graduate Advisor)	Pan Li Assistant Professor of Electrical and Computer Engineering (Committee Member)
Allison Pearson W. L. Giles Distinguished Professor of Management (Minor Graduate Advisor)	James Fowler Associate Professor of Electrical and Computer Engineering (Graduate Coordinator)

Sarah Rajala
Dean of the College of Engineering

Name: Travis Ann Nylin

Date of Degree: December 9, 2011

Institution: Mississippi State University

Major Field: Electrical Engineering

Major Professor: Dr. Erdem Topsakal

Title of Study: BODY CENTRIC ANTENNAS FOR WIRELESS CARDIAC MONITORING

Pages in Study: 59

Candidate for Degree of Master of Science

The overwhelming prevalence of cardiac related deaths is the motivation behind this thesis to develop body centric antennas for wireless cardiac monitoring. Cardiac monitoring can diagnose a number of conditions including: arrhythmia, ischemia, premature atrial complexes, abnormal sinus rhythms, heart blocks, atrial fibrillation, and more. A body centric antenna operating within the ISM band (2.4-2.48GHz) has been designed, simulated, and tested. The simulation and testing indicate low mutual coupling between antennas of varying distances has been achieved. In addition, the simulation and testing indicate that a thin layer of skin over the test subject further reduces mutual coupling.

TABLE OF CONTENTS

Page

LIST OF TABLES iv

LIST OF FIGURES v

CHAPTER

I. INTRODUCTION 1

II. MEASUREMENT TOOLS AND TECHNIQUES 8

Simulation Tools 8
Fabrication Technique 8
Measurement Techniques 9
Antenna Measurement Techniques on Single Antennas 9
Antenna Measurement Techniques on Mannequins 10

III. ANTENNA DESIGN AND TESTING 15

Antenna Design 15
Simulated Antenna Results 16
Fabricated Single Antenna Return Loss Results 17

IV. TORSO SIMULATIONS AND MEASUREMENTS 19

Torso Simulation Design 19
Torso Simulation Return Loss and Near Field Patterns 20
Torso Simulation Mutual Coupling Results 23
Mannequin Testing Results 29
Female Mannequin Return Loss Results 29
Male Mannequin Return Loss Results 35
Female Mannequin Mutual Coupling Results 40
Male Mannequin Mutual Coupling Results 45
Mannequin Testing Mutual Coupling Comparisons 50
Torso Simulation and Mannequin Testing Comparisons 55

V. CONCLUSION AND FUTURE WORK 57

REFERENCES 58

LIST OF TABLES

TABLE Page

1 Distance from each hole to another in cm 11

2 Simulation Hole Distances in centimeters 28

LIST OF FIGURES

FIGURE		Page
1	EKG Signal	2
2	MCL_1 and MCL_6 3-lead configuration	2
3	5-Lead Placement	3
4	12-Lead Placement	4
5	Holter Monitor	4
6	Body Centric Medical Telemetry System Diagram	5
7	Cardio Net MCOT Device [12]	6
8	Corventis Nuvant MCT System [13]	6
9	5 Fabricated Antennas: Patch view (left), Ground Plane View (right)	8
10	Agilent Technologies PNA Network Analyzer	9
11	Set Up For Agilent Network Analyzer Measuring Return Loss.	10
12	Female and Male Mannequins with Holes	11
13	Back of Mannequin with Cutout	12
14	Permittivity of Skin Mimicking Phantom Compared to reference	12
15	Conductivity of Skin Mimicking Phantom Compared to reference	13
16	Female and Male Mannequins with Antennas in Place but No Skin Layer	13
17	Female and Male Mannequins with Skin Layer and Antennas in Place	14
18	HFSS Designed Antenna with Circular Topology	15
19	HFSS Designed Antenna: Profile View	16

20 Return Loss for Simulated Single Antenna 16

21 Single Antenna Far Field Pattern 17

22 Return Loss Measurements Compared to Simulation: (a) S11, (b) S22, (c) S33, (d) S44, (e) S55 18

23 Image of Simulated Torso with Antennas 20

24 Simulated Torso without Skin Return Loss Measurements Compared to Simulated Single Antenna 21

25 Simulated Torso with Skin Return Loss Measurements Compared to Simulated Single Antenna 21

26 Torso Simulation Near-Field Pattern without Skin 22

27 Torso Simulation Near-Field Pattern without Skin 22

28 Mutual Coupling at S1 on Simulated Torso without Skin 23

29 Mutual Coupling at S2 on Simulated Torso without Skin 24

30 Mutual Coupling at S3 on Simulated Torso without Skin 24

31 Mutual Coupling at S4 on Simulated Torso without Skin 25

32 Mutual Coupling at S5 on Simulated Torso without Skin 25

33 Mutual Coupling at S1 on Simulated Torso with Skin 26

34 Mutual Coupling at S2 on Simulated Torso with Skin 26

35 Mutual Coupling at S3 on Simulated Torso with Skin 27

36 Mutual Coupling at S4 on Simulated Torso with Skin 27

37 Mutual Coupling at S5 on Simulated Torso with Skin 28

38 Passive and Active Element Return Loss for S1 on Female without Skin 29

39 Passive and Active Element Return Loss for S2 on Female without Skin 30

40 Passive and Active Element Return Loss for S3 on Female without Skin 31

41 Passive and Active Element Return Loss for S4 on Female without Skin 31

42 Passive and Active Element Return Loss for S5 on Female without Skin 32

43 Passive and Active Element Return Loss for S1 on Female with Skin.....32
44 Passive and Active Element Return Loss for S2 on Female with Skin.....33
45 Passive and Active Element Return Loss for S3 on Female with Skin.....33
46 Passive and Active Element Return Loss for S4 on Female with Skin.....34
47 Passive and Active Element Return Loss for S5 on Female with Skin.....34
48 Passive and Active Element Return Loss for S1 on Male without Skin 35
49 Passive and Active Element Return Loss for S2 on Male without Skin 36
50 Passive and Active Element Return Loss for S3 on Male without Skin 36
51 Passive and Active Element Return Loss for S4 on Male without Skin 37
52 Passive and Active Element Return Loss for S5 on Male without Skin 37
53 Passive and Active Element Return Loss for S1 on Male with Skin 38
54 Passive and Active Element Return Loss for S2 on Male with Skin 38
55 Passive and Active Element Return Loss for S3 on Male with Skin 39
56 Passive and Active Element Return Loss for S4 on Male with Skin 39
57 Passive and Active Element Return Loss for S5 on Male with Skin 40
58 Mutual Coupling with S1 for Female without Skin 41
59 Mutual Coupling with S2 for Female without Skin 41
60 Mutual Coupling with S3 for Female without Skin 42
61 Mutual Coupling with S4 for Female without Skin 42
62 Mutual Coupling with S5 for Female without Skin 43
63 Mutual Coupling with S1 for Female with Skin 43
64 Mutual Coupling with S2 for Female with Skin 44
65 Mutual Coupling with S3 for Female with Skin 44
66 Mutual Coupling with S4 for Female with Skin 45
67 Mutual Coupling with S5 for Female with Skin 45

68 Mutual Coupling with S1 for Male without Skin....46
69 Mutual Coupling with S2 for Male without Skin....46
70 Mutual Coupling with S3 for Male without Skin....47
71 Mutual Coupling with S4 for Male without Skin....47
72 Mutual Coupling with S5 for Male without Skin....48
73 Mutual Coupling with S1 for Male with Skin....48
74 Mutual Coupling with S2 for Male with Skin....49
75 Mutual Coupling with S3 for Male with Skin....49
76 Mutual Coupling with S4 for Male with Skin....50
77 Mutual Coupling with S5 for Male with Skin....50
78 Mutual Coupling Skin/No Skin Comparison with S12 for Female....51
79 Mutual Coupling Skin/No Skin Comparison with S13 for Female....52
80 Mutual Coupling Skin/No Skin Comparison with S14 for Female....52
81 Mutual Coupling Skin/No Skin Comparison with S15 for Female....53
82 Mutual Coupling Skin/No Skin Comparison with S12 for Male....53
83 Mutual Coupling Skin/No Skin Comparison with S13 for Male....54
84 Mutual Coupling Skin/No Skin Comparison with S14 for Mal....54
85 Mutual Coupling Skin/No Skin Comparison with S15 for Male....55
86 Mutual coupling of the simulated torso with the male mannequin without skin....56
87 Mutual coupling of the simulated torso with the male mannequin with skin....56

CHAPTER I

INTRODUCTION

The main motivation behind designing continuous cardiac monitoring technologies in this thesis is the overwhelming number of lives affected by heart disease. In 2006, heart disease was the number one killer of men and women in the U.S., claiming over 831,000 lives. Heart disease kills one out of four people in the U.S. and more than 81 million people in the U.S. experience some form of heart disease. The key to saving the lives of victims of heart disease is early action and accurate diagnostics, since only 27% of people are aware of the main symptoms of a heart attack [1].

Cardiac monitoring is the continuous observation of a patient's cardiac function using techniques such as oscilloscope readings, electrocardiogram, or audible recording of heart rhythm. Generally, the cardiac monitoring system is equipped with an alarm system to alert medical staff of potential cardiac abnormalities, which include but are not limited to: arrhythmia, premature atrial complexes, abnormal sinus rhythms, heart blocks, atrial fibrillation, bundle branch block, ischemia, ventricular tachycardia (VT), and supraventricular tachycardia (SVT) [2, 3, 4].

The preferred method of monitoring abnormalities is with an electrocardiogram (EKG), which measures the electrical activity of the heart. Electrodes are placed in specific locations on the body and pick up electrical signals from the heart, which consists of four waves, P, QRS, T, and U. Each of these waves provides different

information about the hearts function, which aids in the diagnostic process [4, 5]. A typical EKG signal is shown in Figure 1 [6].

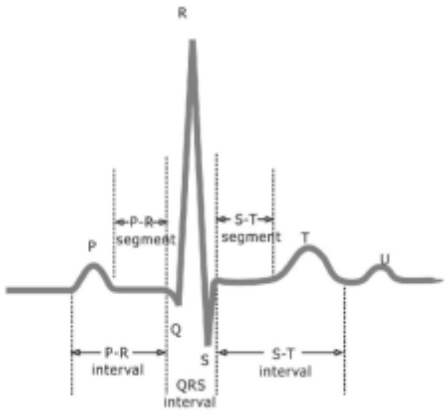

Figure 1 EKG Signal

The placement of the electrode leads is an integral part of cardiac monitoring through EKG, and there are certain configurations that are used to diagnose different abnormalities. The most common types are MCL_1, MCL_6, V_1, V_6, and 12-lead placement. MCL_1 and MCL_6 are measured using a 3- lead system where the placement is done as shown in Figure 2 [7].

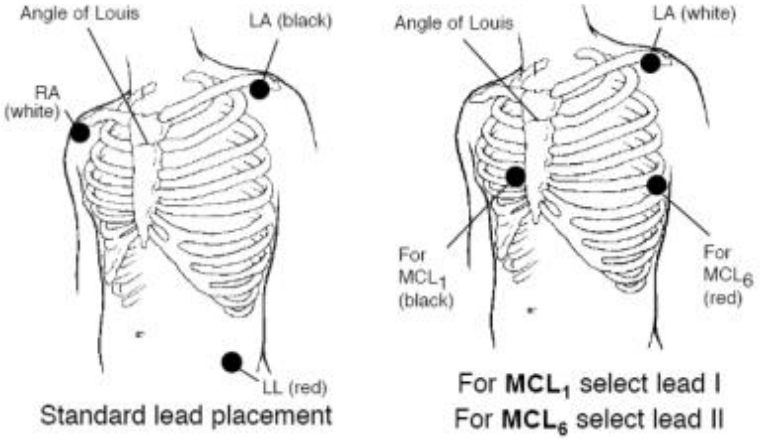

Figure 2 MCL_1 and MCL_6 3-lead configuration

This configuration is good for differentiating wide QRS rhythms. Some research suggests that MCL_1 and MCL_6 might be a substitution for V_1 and V_6 configurations, which require 5-leads. However, when a patient experiences ventricular tachycardia, V_1 and V_6 configurations are preferred because MCL_1 and MCL_6 have detection accuracy around 61%. V_1 and V_6 configurations are shown in Figure 3 [7].

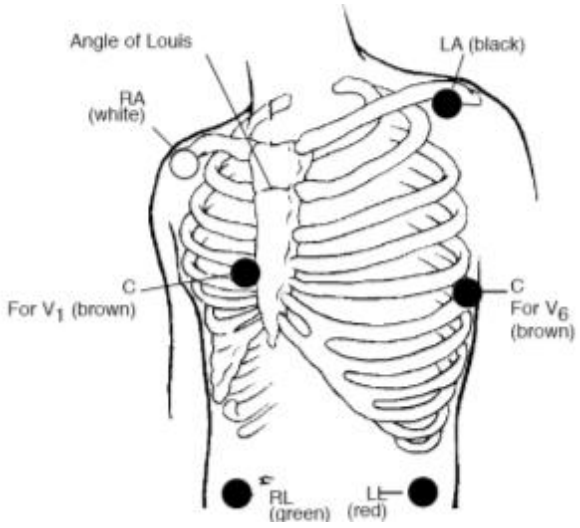

Figure 3 5-Lead Placement

On the other hand, 12-lead systems, shown in Figure 4, are said to be the most preferred configuration because it provides a more global view of cardiac function [3, 4, 7]. Regardless of configuration, the electric signal captured is sent via wires that connect the electrodes to a bedside or nurse station monitor [5].

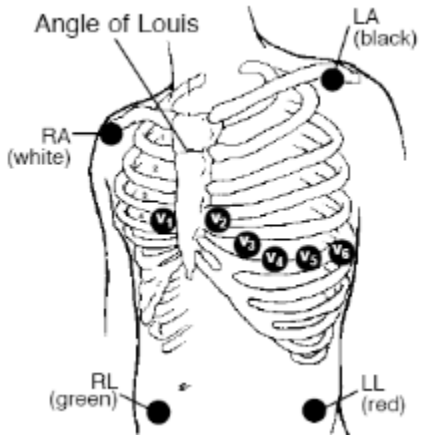

Figure 4 12-Lead Placement

In certain cases, a Holter Monitoring system is used for long term monitoring of the patient's performance. The Holter monitor is worn somewhere between 24hours – up to a month and contains between 3-8 electrodes which are placed at strategic locations on the upper body [8, 9]. A common electrode placement is shown in Figure 5.

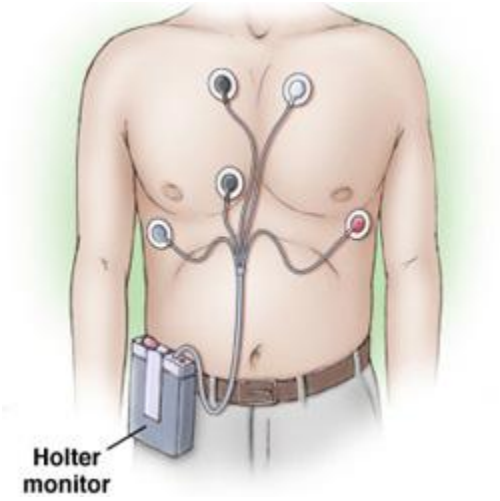

Figure 5 Holter Monitor

These electrodes are connected by wires to a recording device that is worn around the neck or in a pocket [10]. The recorded signals are analyzed and matched to a diary

kept by the patient. This method is used to diagnose and detect heart problems such as sick sinus syndrome, heart arrhythmias, and myocardial ischemia [8, 9]. To minimize patient discomfort and eliminate the need for wired electrodes, an alternative is to use a body centric system combined with wireless telemetry to send patient information from the body to the monitoring stations. In general, body centric medical telemetry systems are used to monitor a variety of patient information [11]. As shown in Figure 6, a body centric system is placed on the body that wirelessly communicates to a receiver that is either worn by the patient or near the patient on a bed side table. That receiver could then send a wireless signal to the monitoring station, where medical staff could monitor patient vitals. This type of configuration is useful in typical hospital settings for EKG or at home Holter monitoring stations.

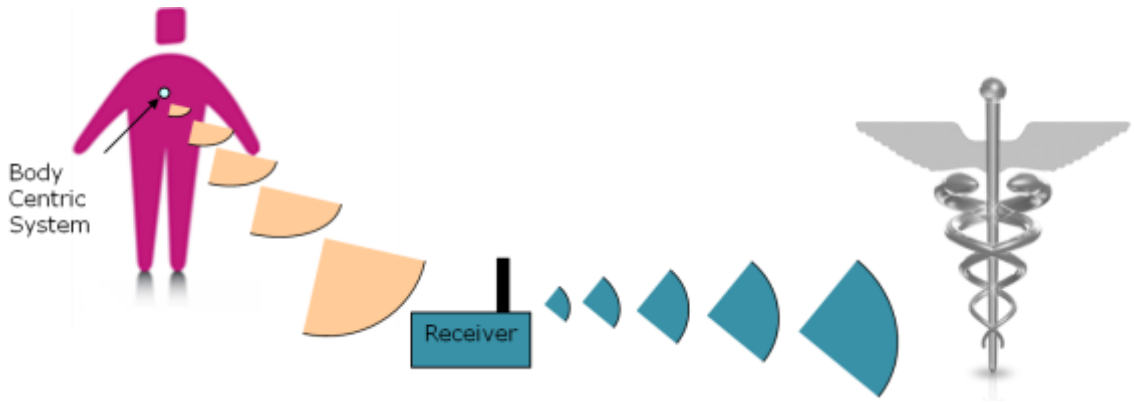

Figure 6 Body Centric Medical Telemetry System Diagram

Current industry body centric devices designed to minimize wires have include the Cardio Net MCOT and Corventis Nuvant MCT System. The Cardio Net MCOT system, as shown in Figure 7, consists of three electrodes, a neck worn device, and a handheld transceiver.

Figure 7 Cardio Net MCOT Device [12]

The electrodes collect patient cardiac information and then send the data through wires to the neck worn transmitter. The transmitter communicates the critical information to the hand held transceiver, which in turn sends the data to the Cardio Net monitoring center. While this system does aim to improve patient mobility and comfort, it fails to completely eliminate the need for wires.

On the other hand, the Corventis Nuvant MCT System, shown in Figure 8, does eliminate wires. This system works as an ambulance arrhythmia monitor that is affixed to the chest of a patient during transport to the hospital.

Figure 8 Corventis Nuvant MCT System [13]

The critical information is sent to the Corventis monitoring center and physicians are notified of patient condition. While arrhythmia is one important cardiac condition to

monitor, there are other important conditions to monitor, most of which require a multi lead monitoring system.

This research aims to develop a body centric antenna for wireless cardiac monitoring. The goals of this study include: antenna design, on torso simulation, and on mannequin simulation. The design of the prototype antenna is confined to the size parameters of current EKG electrodes, which are 4.76cm, in order to minimize patient discomfort. Also, an operating frequency of between 2.4GHz and 2.48GHz allows the antenna to communicate via the ISM band to a bed side or room unit. The simulation of the designed antenna is of a simulated torso with an array configuration similar to that of common Holter monitor placement where mutual coupling and field distribution are analyzed. Mannequin testing of the same Holter monitor configuration used in simulations is done to mimic the contours of the human body and analyze mutual coupling in this environment.

CHAPTER II

MEASUREMENT TOOLS AND TECHNIQUES

Simulation Tools

Ansys HFSS was used to design and simulate the single antenna and the simulated torso. HFSS is a 3D full-wave electromagnetic field simulation tool that solves user specified geometries, materials, and desired output using a finite element method.

Fabrication Technique

To test the antenna designed in HFSS, a Protomat S62 milling machine was used to mill five antennas. Holes were drilled in the feed location of each of the antennas and coaxial cables were soldered into place. The final fabricated antennas are shown in Figure 9 with the patch topology shown left and the ground plane shown right.

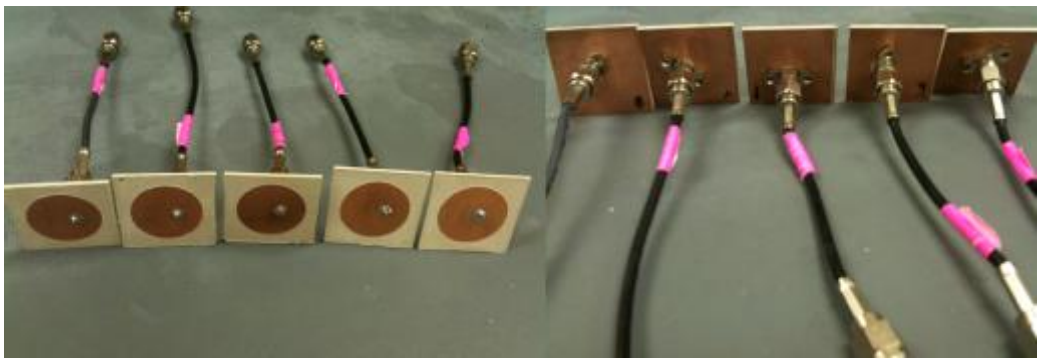

Figure 9 5 Fabricated Antennas: Patch view (left), Ground Plane View (right)

Measurement Techniques

Antenna Measurement Techniques on Single Antennas

The measurement of fabricated antennas was done using Agilent Technologies PNA Network Analyzer, which is shown in Figure 10. The Agilent 85052 B 3.6mm Calibration Kit was used to calibrate the system before measuring the antennas. Measurement of the antennas was done in open air as shown in Figure 11.

Figure 10 Agilent Technologies PNA Network Analyzer

Figure 11 Set Up For Agilent Network Analyzer Measuring Return Loss.

Antenna Measurement Techniques on Mannequins

To test the antennas in the Holter Monitor locations, both female and male mannequins were used. The permittivity measured 3, while the conductivity was 0.0114. Holes were drilled in the mannequins mimicking the appropriate five electrode placement for the Holter Monitor.

Table 1 details the distance from each hole to another. The male (left) and female (right) mannequins with the holes drilled are shown in Figure 12 along with the names of each hole.

Table 1 Distance from each hole to another in cm

	Male					Female				
	S1	S2	S3	S4	S5	S1	S2	S3	S4	S5
S1		13.0	16.8	27.5	31.6		10.0	15.4	25.9	27.8
S2			16.0	30.7	26.4			16.3	28.2	26.1
S3				15.4	16.5				12.5	13.9
S4					19.1					16.8

Figure 12 Female and Male Mannequins with Holes

A large rectangular cutout was removed from the back of the mannequins as shown in Figure 13, to allow easy access to the network analyzer cables and the antenna coaxial cables.

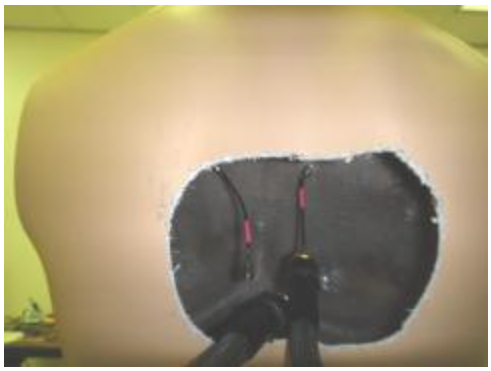

Figure 13 Back of Mannequin with Cutout

A rectangular slab of phantom skin was fabricated to place over each of the mannequins to test the antennas on top of a skin layer. The average depth of the skin layer is 1.6mm. The permittivity and conductivity of the skin phantom are shown in Figure 14 and Figure 15: Conductivity of Skin Mimicking Phantom Compared to reference, respectively. These phantoms were created from a mixture of water, gelatin A, and oil [14].

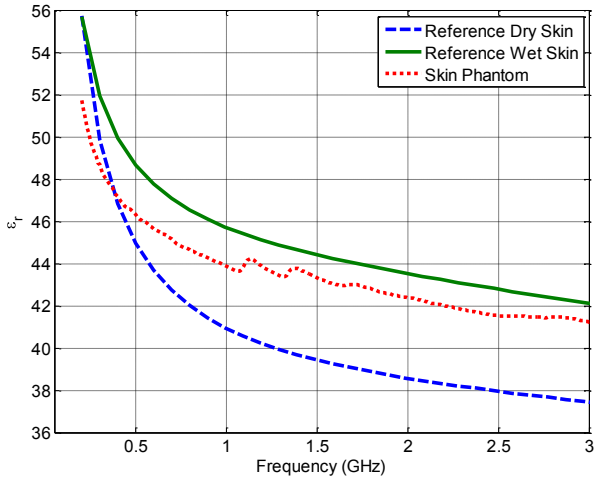

Figure 14 Permittivity of Skin Mimicking Phantom Compared to reference

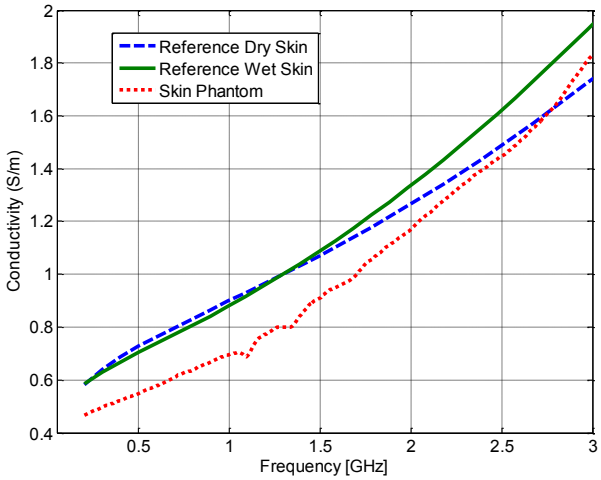

Figure 15 Conductivity of Skin Mimicking Phantom Compared to reference

Figure 16 is an image of the female and male mannequins without skin, but with the antennas in place for measurement. Figure 17 is an image of the female and male mannequins with the skin layers on and the antennas in place.

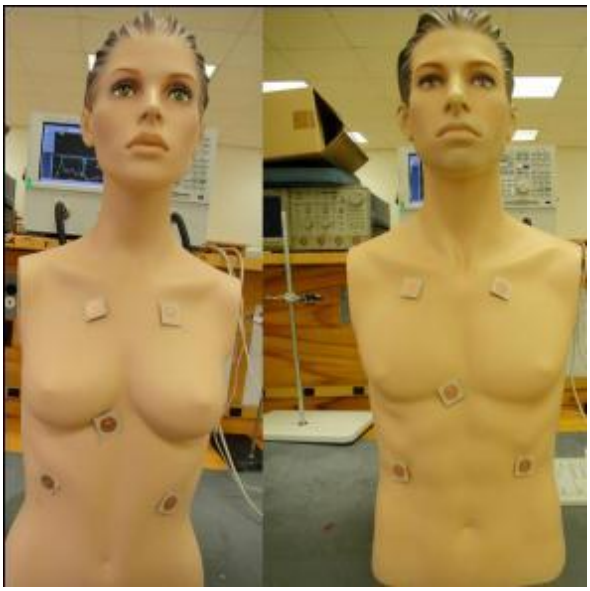

Figure 16 Female and Male Mannequins with Antennas in Place but No Skin Layer

Figure 17 Female and Male Mannequins with Skin Layer and Antennas in Place

The antennas were connected to the network analyzer one by one and the return loss of each of the antennas was recorded, while all other antennas remained passive. The return loss of each antenna was also measured with the each of the other antennas receiving signal from the network analyzer, one by one. For example, the return loss was measured for S1 while S2 was connected to the network analyzer. Then S11 was measured while S3 was connected. This process was repeated for each of the positions. This test was repeated for both male and female mannequins with and without skin.

CHAPTER III

ANTENNA DESIGN AND TESTING

Antenna Design

The antenna is comprised of three layers: patch topology, substrate, and ground plane. The patch topology of the antenna, shown in Figure 18, is a symmetrical, circular design so that the orientation of the antenna would not introduce variance during testing.

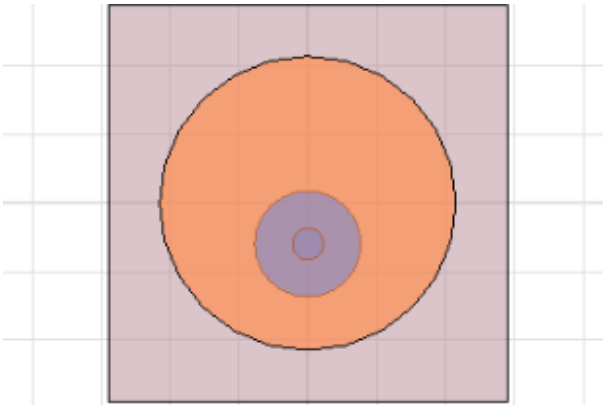

Figure 18 HFSS Designed Antenna with Circular Topology

The circular patch has a radius of 1.075cm with the center of the feed located 0.297cm from the center of the patch. The substrate and ground plane of the antenna measure 2.9cm x 2.9cm. The substrate, with a thickness of 1.27mm, is Rogers RO3010. Figure 19 shows a profile view of the antenna.

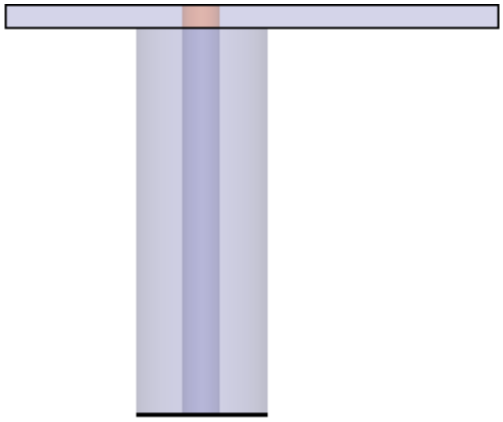

Figure 19 HFSS Designed Antenna: Profile View

Simulated Antenna Results

The results of the simulated single antenna are shown in the following Figures. Figure 20 shows the resulting return loss for the antenna to be --14dB within ISM band and a bandwidth of 24MHz. Figure 21 shows the far field pattern.

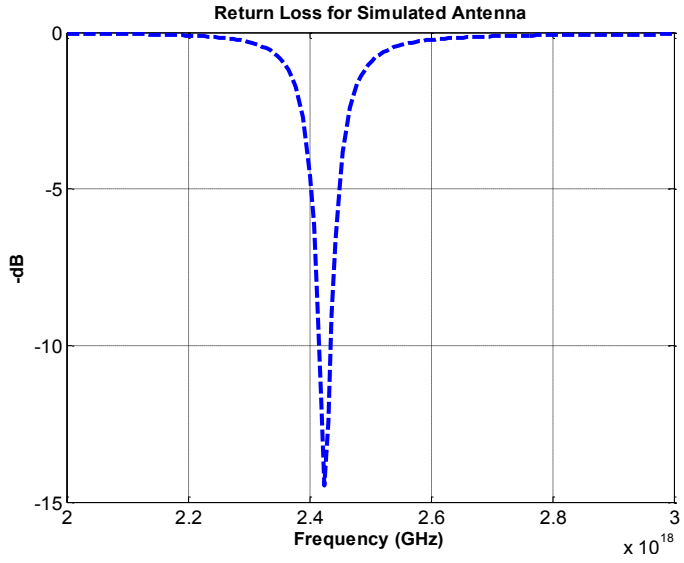

Figure 20 Return Loss for Simulated Single Antenna

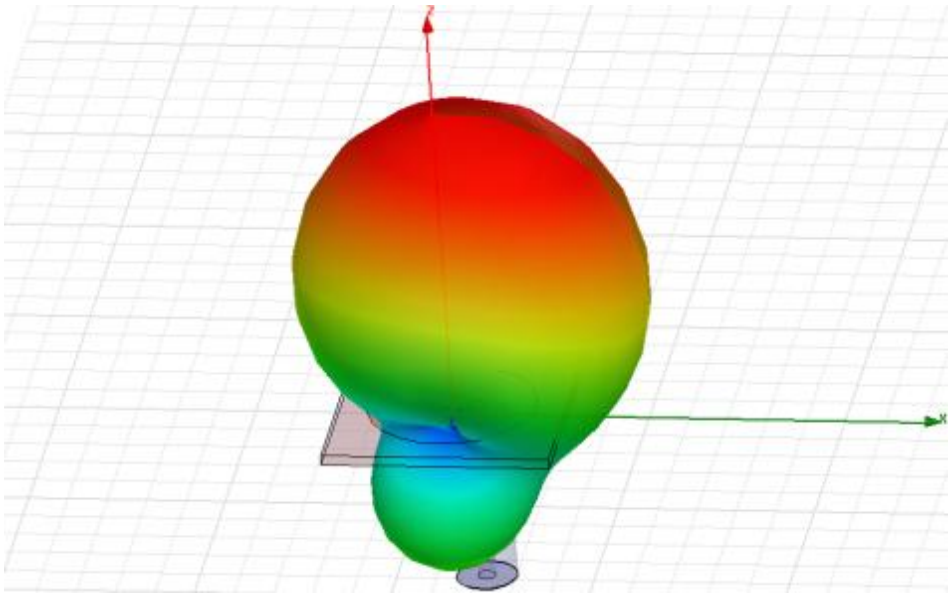

Figure 21 Single Antenna Far Field Pattern

Fabricated Single Antenna Return Loss Results

Each antenna was named by its future location on the test mannequins, S1-S5, and the return loss each of the five antennas was measured. In Figure 22 (a), the return loss for Antenna S1 is -15dB within ISM band. In Figure 22 (b), the return loss for Antenna S2 is -14dB within ISM band. In Figure 22 (c), the return loss for Antenna S3 is -26dB within ISM band. In Figure 22 (d), the return loss for Antenna S4 is -23dB within ISM band. In Figure 22 (e), the return loss for Antenna S5 is -20dB within ISM band.

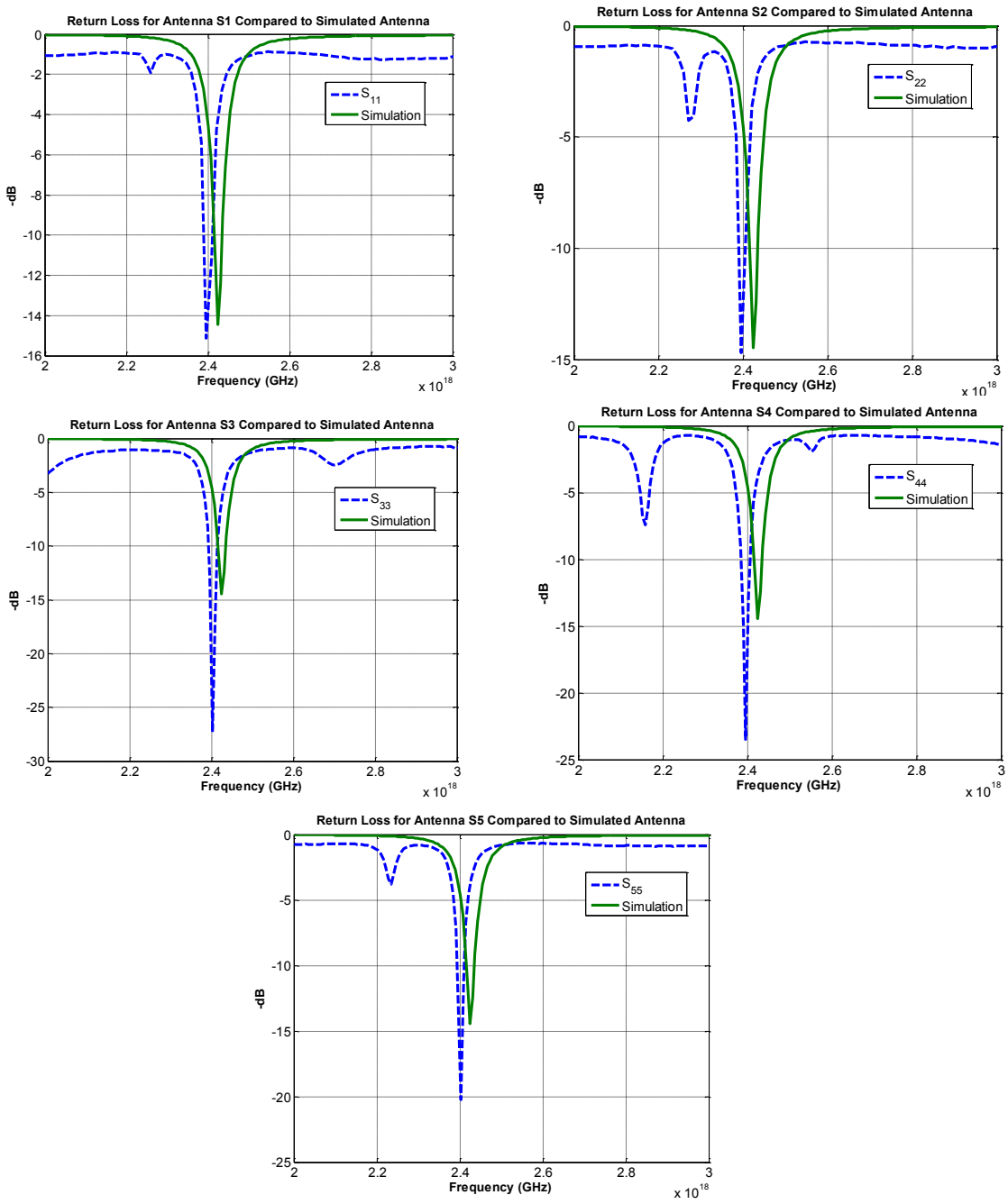

Figure 22 Return Loss Measurements Compared to Simulation: (a) S11, (b) S22, (c) S33, (d) S44, (e) S55

CHAPTER IV

TORSO SIMULATIONS AND MEASUREMENTS

Torso Simulation Design

To simulate physical testing of the Holter monitor array on test mannequins, HFSS was used to build a simulated mannequin abdomen model as seen in Figure 23. This model was based on the physical measurements of the male mannequin used during testing. The circumference of the mannequin at the widest part was 99cm. An open ended cylinder with radius 15.76cm was used to represent the torso. In addition, 10mm holes were cut out of the cylinder in the location of the Holter Monitor electrodes. Next, five identical patch antennas as designed in the previous chapter, were placed inside the holes. Covering the front have of the cylinder is a 1.6mm layer of skin, whose electromagnetic properties match that of human skin.

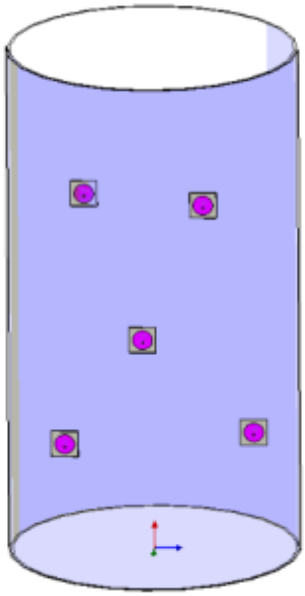

Figure 23 Image of Simulated Torso with Antennas

Torso Simulation Return Loss and Near Field Patterns

The HFSS torso design was simulated with all antennas with and without the skin layer. The return loss and mutual coupling are examined for all antenna pairs. The return loss for each of the antennas in the simulation without skin was compared to the simulated single antenna design as shown in Figure 24. The return loss values range from -11dB to -12dB at ISM band.

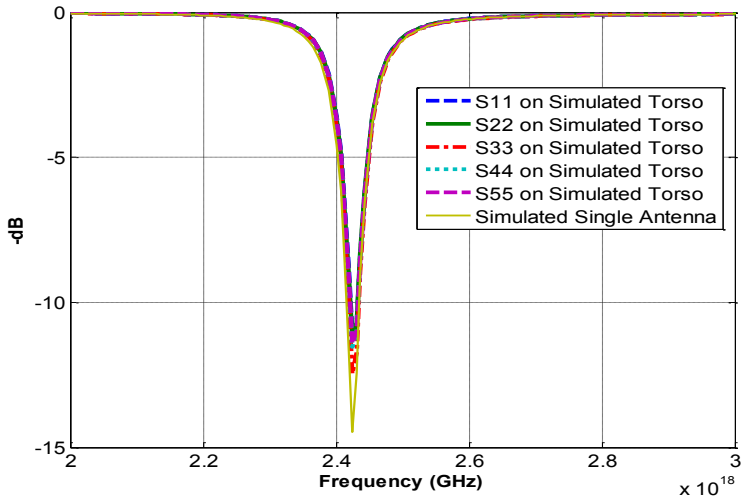

Figure 24 Simulated Torso without Skin Return Loss Measurements Compared to Simulated Single Antenna

Figure 25 shows the return loss for each of the antennas in the simulation with skin. The return loss values range from -10dB to -21dB within ISM band.

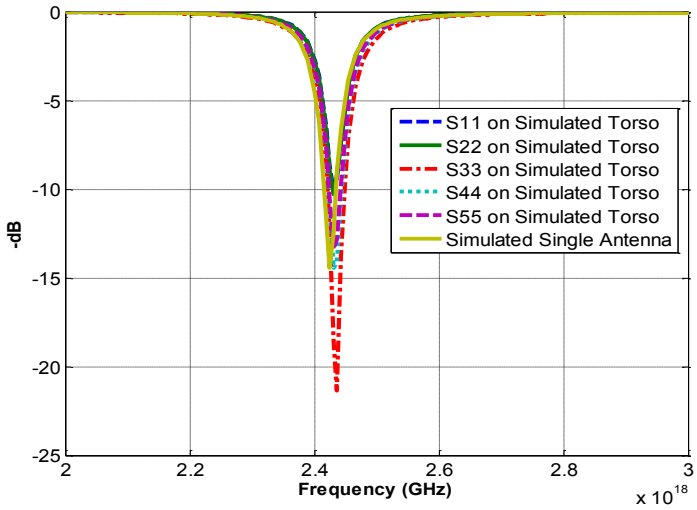

Figure 25 Simulated Torso with Skin Return Loss Measurements Compared to Simulated Single Antenna

The near field patterns are shown in Figures 26 and 27. Figure 26 is the near field pattern without skin, while Figure 27 is with skin.

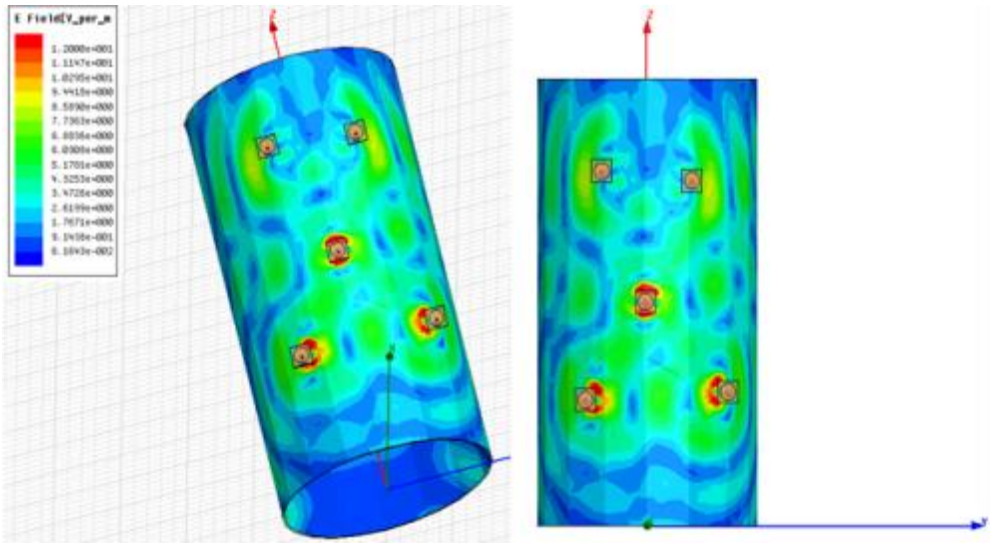

Figure 26 Torso Simulation Near-Field Pattern without Skin

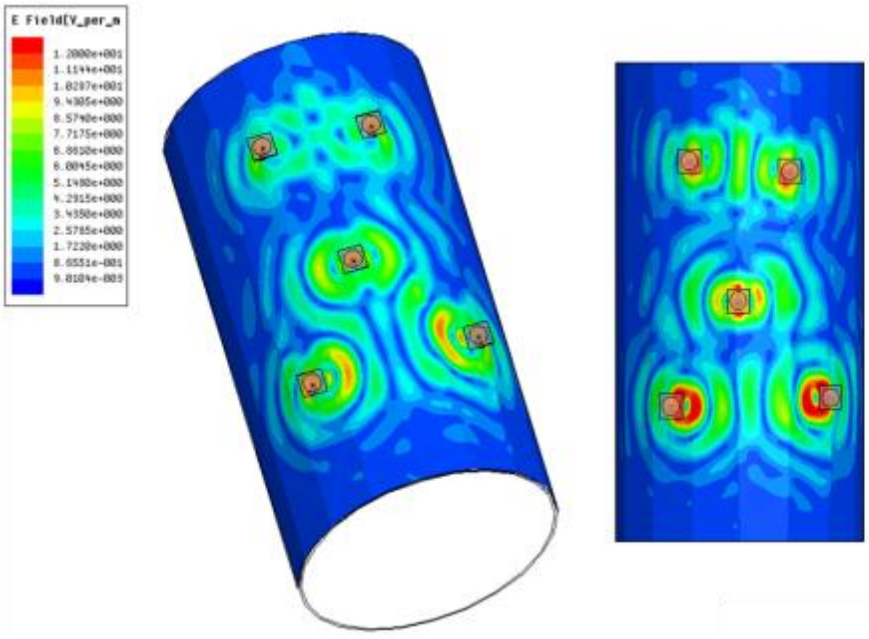

Figure 27 Torso Simulation Near-Field Pattern without Skin

Torso Simulation Mutual Coupling Results

Figures 28-32 are the results for mutual coupling for the simulated torso without skin. In Figure 28, the mutual coupling between S1 and the other elements ranges from -33dB to -44dB.

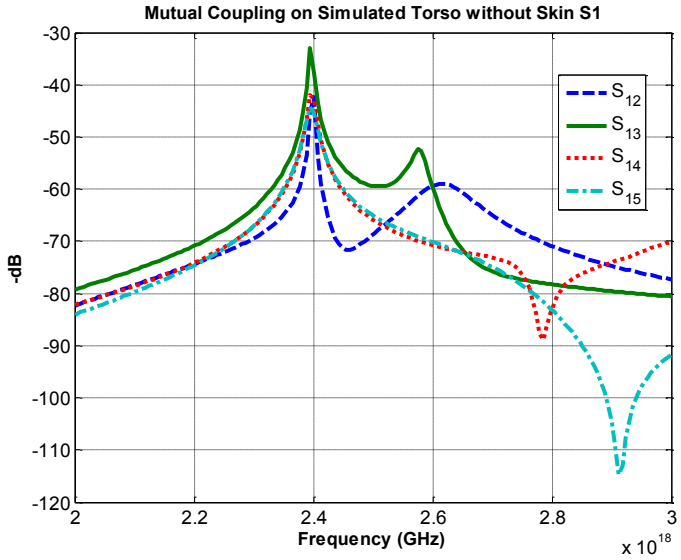

Figure 28 Mutual Coupling at S1 on Simulated Torso without Skin

In Figure 29, the mutual coupling between S2 and the other elements ranges from -29dB to -46dB.

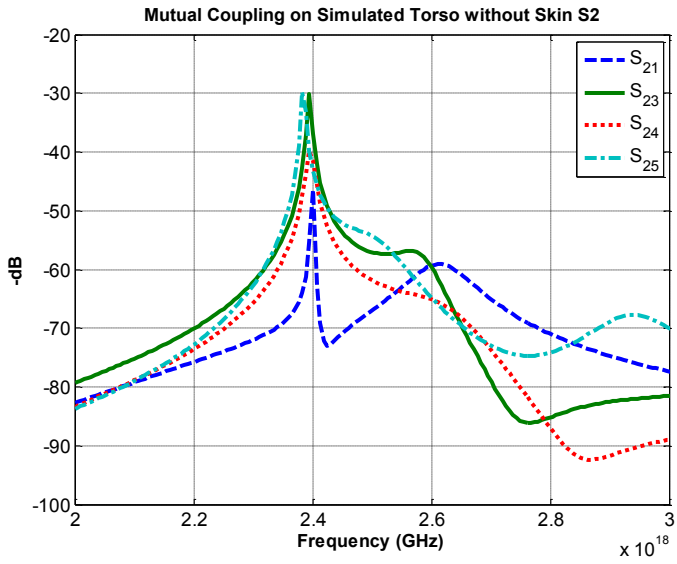

Figure 29 Mutual Coupling at S2 on Simulated Torso without Skin

In Figure 30, the mutual coupling between S3 and the other elements ranges from -30dB to -33dB.

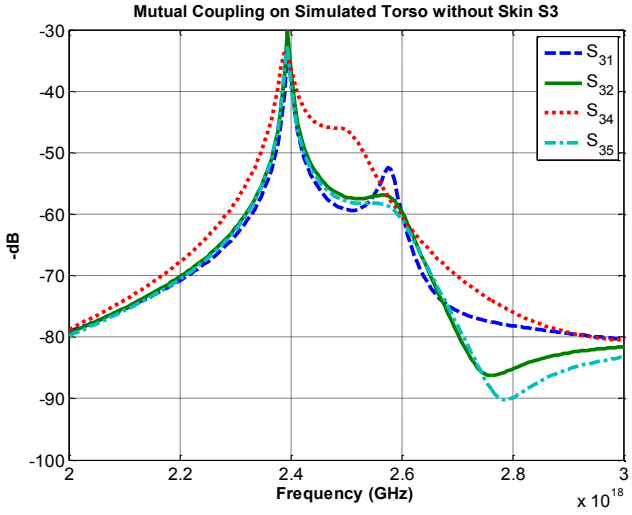

Figure 30 Mutual Coupling at S3 on Simulated Torso without Skin

In Figure 31, the mutual coupling between S4 and the other elements ranges from -33dB to -43dB.

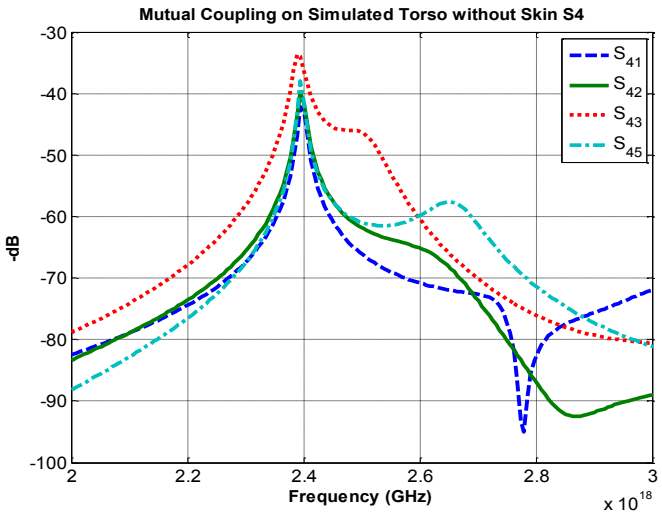

Figure 31 Mutual Coupling at S4 on Simulated Torso without Skin

In Figure 32, the mutual coupling between S5 and the other elements is ranges from -32dB to -44dB.

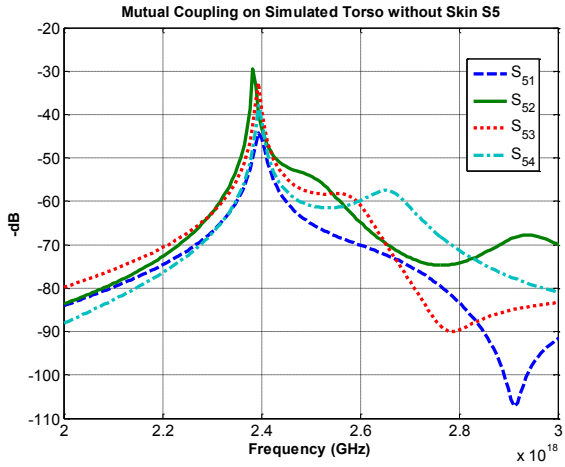

Figure 32 Mutual Coupling at S5 on Simulated Torso without Skin

Figures 33-37 are the results for the simulated torso with the skin layer. In Figure 33, the mutual coupling between S1 and the other elements ranges from -34dB to -50dB within ISM band.

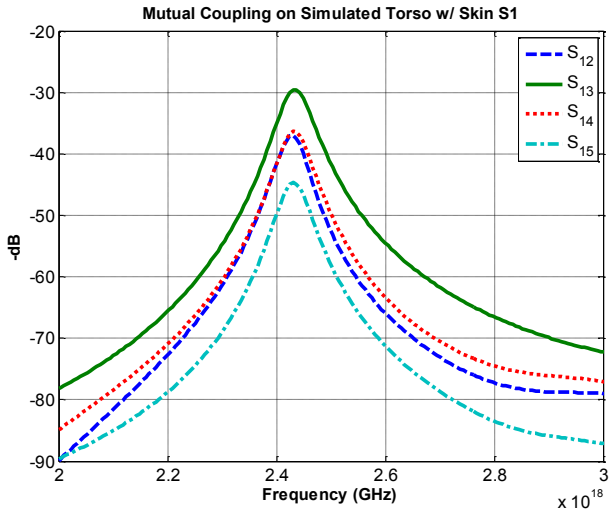

Figure 33 Mutual Coupling at S1 on Simulated Torso with Skin

In Figure 34, the mutual coupling between S2 and the other elements ranges from -35dB to -44dB within ISM band.

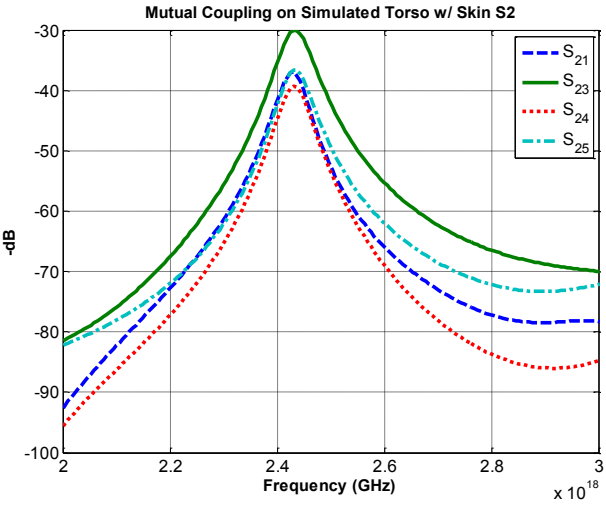

Figure 34 Mutual Coupling at S2 on Simulated Torso with Skin

In Figure 35, the mutual coupling between S3 and the other elements ranges from -35dB to -44dB within ISM band.

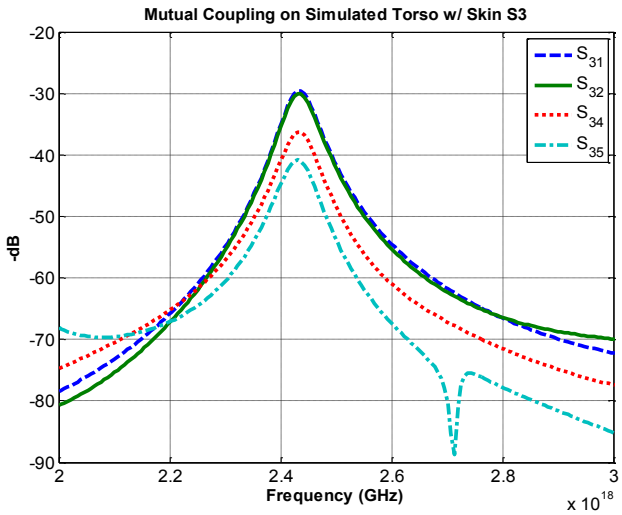

Figure 35 Mutual Coupling at S3 on Simulated Torso with Skin

In Figure 36, the mutual coupling between S4 and the other elements ranges from -42dB to -52dB within ISM band.

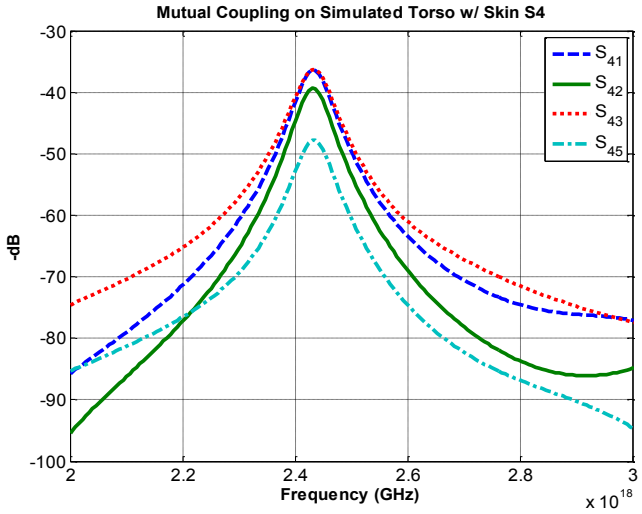

Figure 36 Mutual Coupling at S4 on Simulated Torso with Skin

In Figure 37, the mutual coupling between S5 and the other elements is ranges from -42dB to -52dB within ISM band.

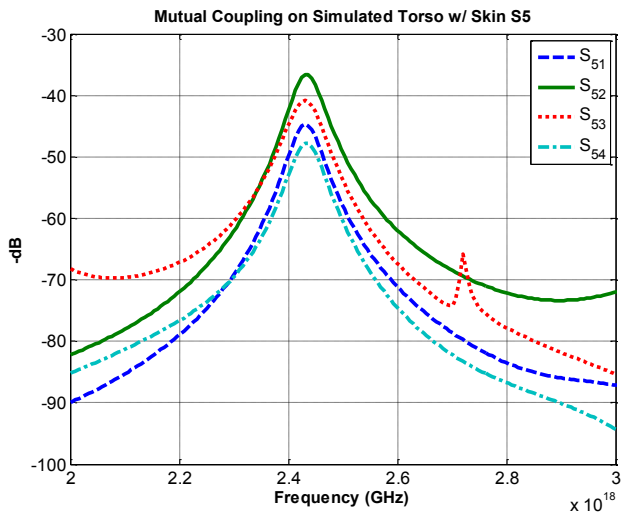

Figure 37 Mutual Coupling at S5 on Simulated Torso with Skin

Theoretically, the mutual coupling should be highest when the antennas are closest together and lowest when they are farthest apart. Table 2 shows the distance from one hole to another on the simulations. These values are the same as those on the male mannequin with a maximum at 31.6cm and minimum at 13.0cm.

Table 2 Simulation Hole Distances in centimeters

	S1	S2	S3	S4	S5
S1		13.0	16.8	27.5	31.6
S2			16.0	30.7	26.4
S3				15.4	16.5
S4					19.1

After analyzing the simulations with the skin and without the skin layer, it is evident that there are three major differences between the two. First, the simulation with the skin has the mutual coupling peaks slightly different from that without skin. The second major difference is that the simulation without skin has at least one corresponding maximum and minimum mutual coupling value and hole distance at S15 and S12,

respectively. However, the mutual coupling values and hole distances do not correspond for the simulation with the skin layer. Thirdly, the simulation with the skin has a more gradual peak to maximum mutual coupling when compared to the sharp peak of the simulation without a skin layer. This combined with the fact that the simulation with a skin layer has slightly lower mutual coupling values than that of the simulation without skin, suggests that skin layer may lessen mutual coupling.

Mannequin Testing Results

Female Mannequin Return Loss Results

Figures 38-42 show the results for the female mannequin without skin. In Figure 38, the return loss for Antenna S1 is -15dB within ISM band when all other elements are passive, and between -14dB and -15dB when each of the other antennas is active.

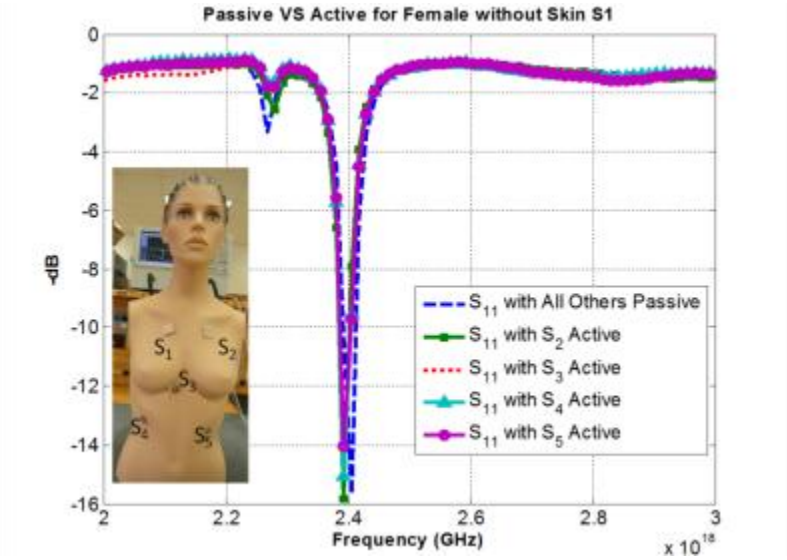

Figure 38 Passive and Active Element Return Loss for S1 on Female without Skin

In Figure 39, the return loss for Antenna S2 is -19dB within ISM band when all other elements are passive, and between -14dB and-18dB when each of the other elements is active.

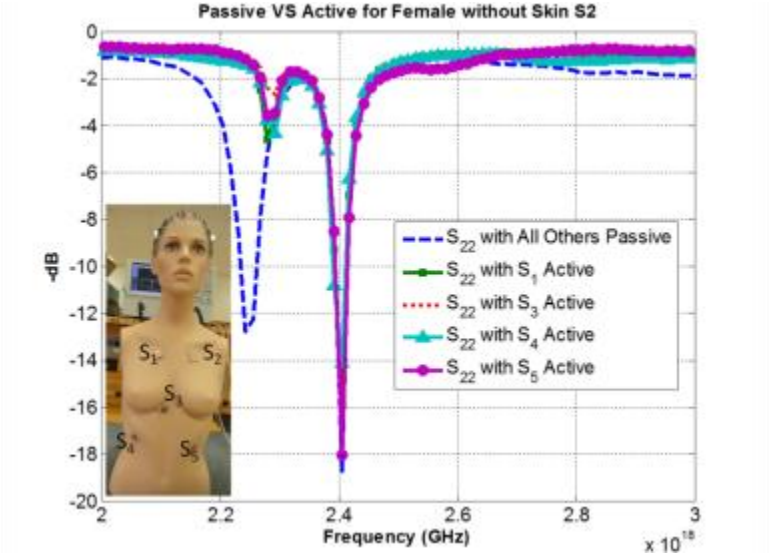

Figure 39 Passive and Active Element Return Loss for S2 on Female without Skin

In Figure 40, the return loss for Antenna S3 is -25dB within ISM band when all other elements are passive, and between -10dB and -26dB when each of the other elements is active.

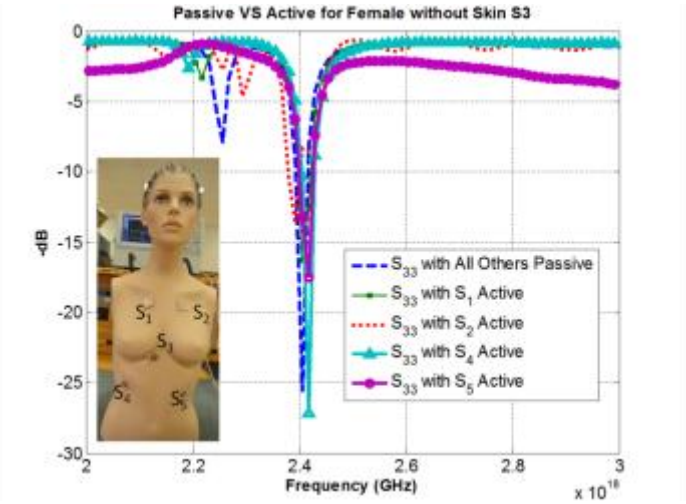

Figure 40 Passive and Active Element Return Loss for S3 on Female without Skin

In Figure 41, the return loss for Antenna S4 is -11dB within ISM band when all other elements are passive, and between -12dB and -14dB when each of the other elements is active.

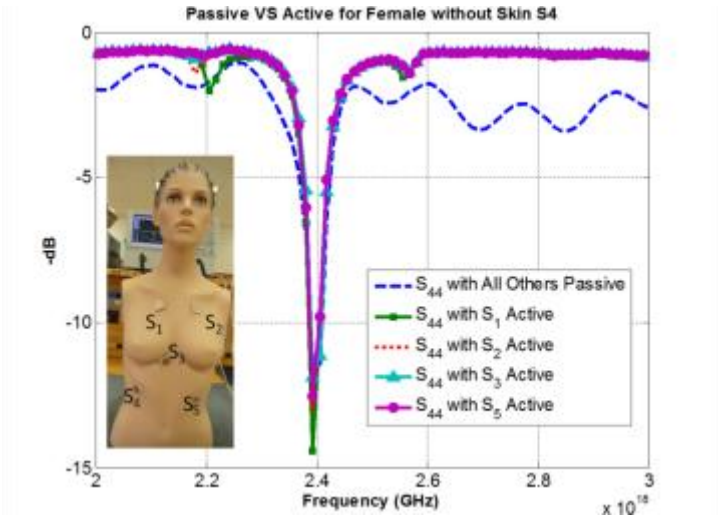

Figure 41 Passive and Active Element Return Loss for S4 on Female without Skin

In Figure 42, the return loss for Antenna S5 is -18dB within ISM band when all other elements are passive, and between -8dB and -19dB when each of the other elements is active.

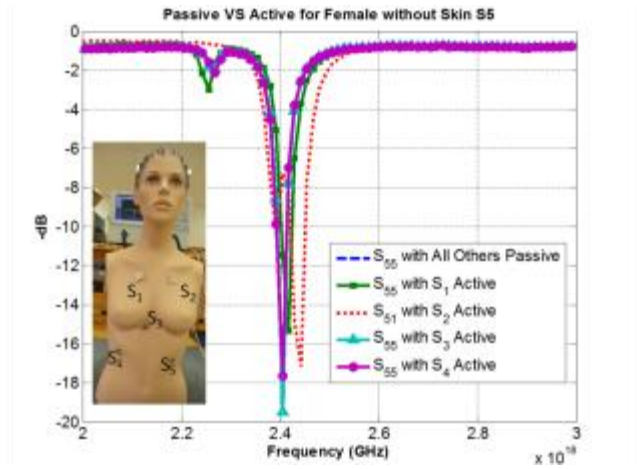

Figure 42 Passive and Active Element Return Loss for S5 on Female without Skin

Figures 43-47 show the results for the female mannequin with skin. In Figure 43, the return loss for Antenna S1 is -15dB within ISM band when all other elements are passive, and between -14dB and -15dB when each of the other antennas is active.

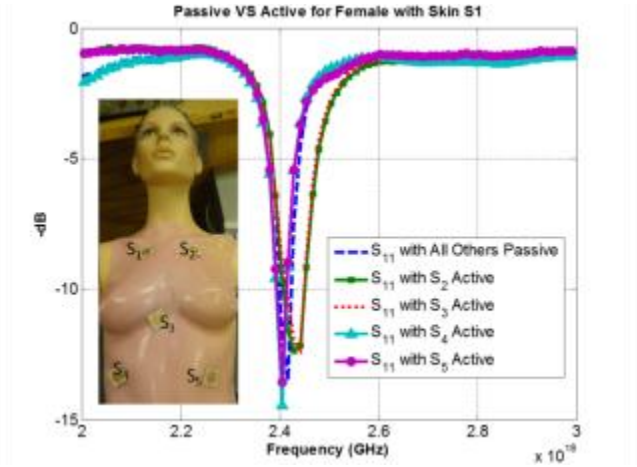

Figure 43 Passive and Active Element Return Loss for S1 on Female with Skin

In Figure 44, the return loss for Antenna S2 is -12dB within ISM band when all other elements are passive, and between -9dB and-14dB when each of the other elements are active.

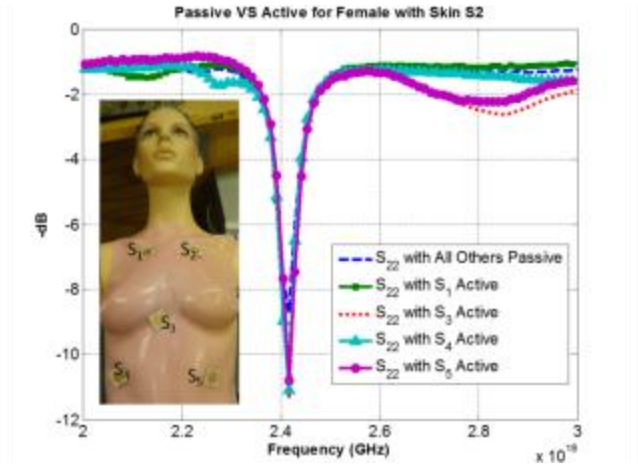

Figure 44 Passive and Active Element Return Loss for S2 on Female with Skin

In Figure 45, the return loss for Antenna S3 is -10dB within ISM band when all other elements are passive, however it is -24dB within ISM band. All of the other S3 return loss measurements with S3 active were shifted to the right as well between -19dB and -25dB when each of the other elements are active.

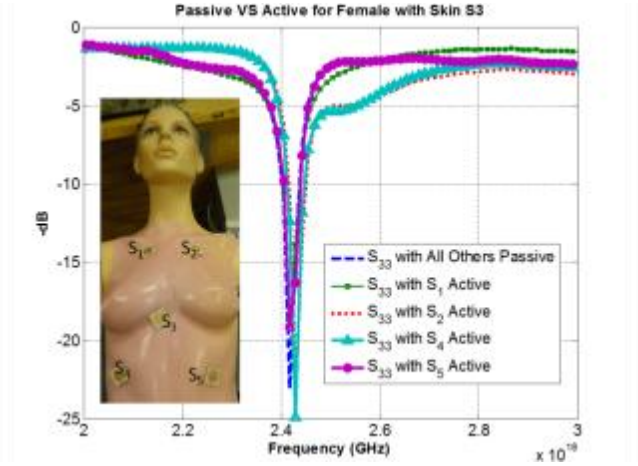

Figure 45 Passive and Active Element Return Loss for S3 on Female with Skin

In Figure 46, the return loss for Antenna S4 is -11dB within ISM band when all other elements are passive, and between -11dB and -15dB when each of the other elements is active.

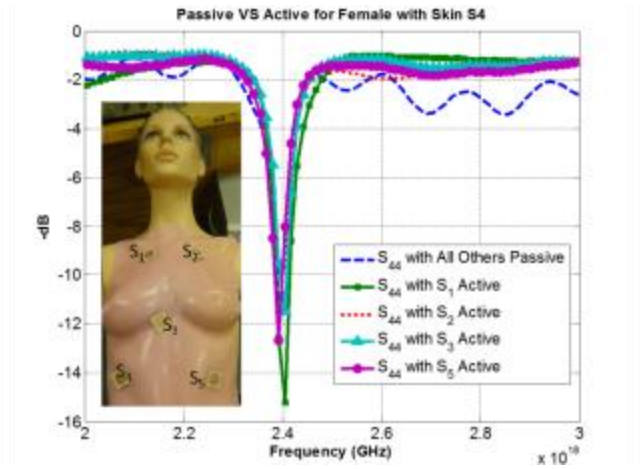

Figure 46 Passive and Active Element Return Loss for S4 on Female with Skin

In Figure 47, the return loss for Antenna S5 is -13dB within ISM band when all other elements are passive, and between -7dB and -15dB when each of the other elements is active.

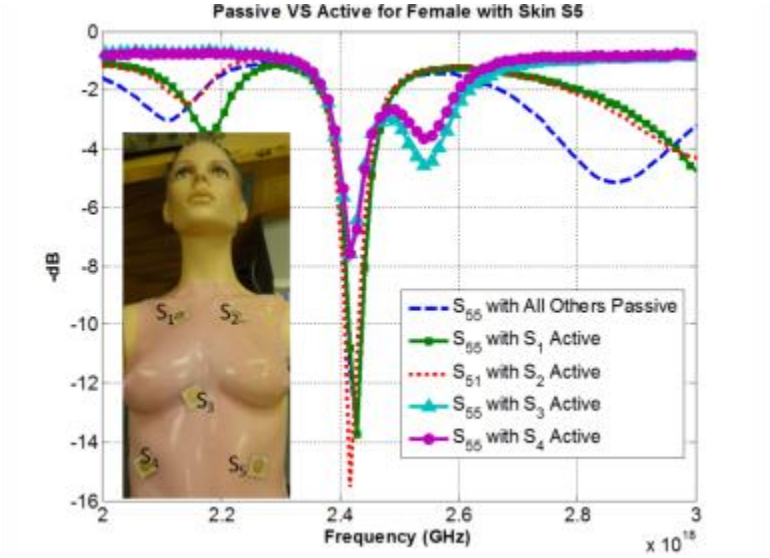

Figure 47 Passive and Active Element Return Loss for S5 on Female with Skin

Male Mannequin Return Loss Results

Figures 48-52 show the results for the male mannequin without skin. In 48, the return loss for Antenna S1 is -18dB within ISM band when all other elements are passive, and between -18dB and -37dB when each of the other antennas is active.

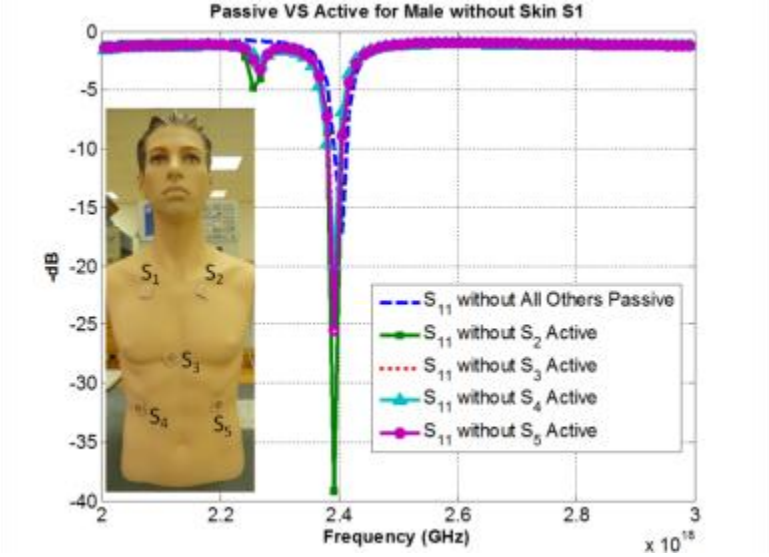

Figure 48 Passive and Active Element Return Loss for S1 on Male without Skin

In Figure 49, the return loss for Antenna S2 is -13dB within ISM band when all other elements are passive, and between -12dB and-13dB when each of the other elements are active.

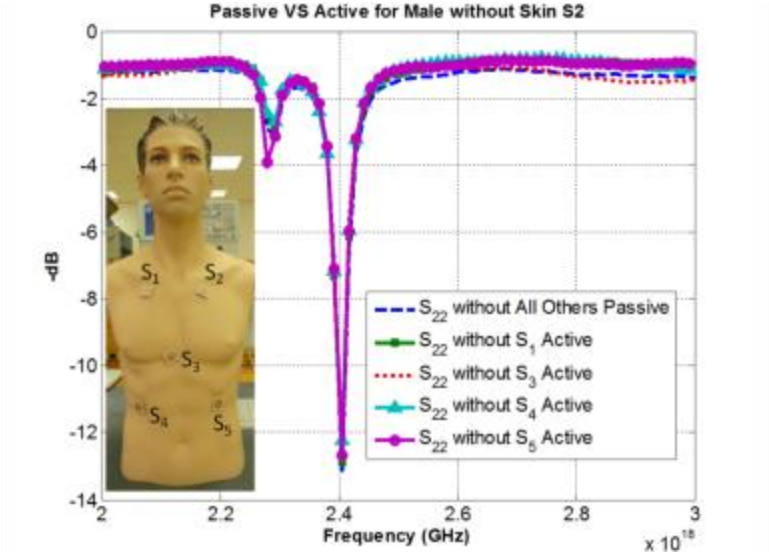

Figure 49 Passive and Active Element Return Loss for S2 on Male without Skin

In Figure 50, the return loss for Antenna S3 is -16dB within ISM band when all other elements are passive, and between -15dB and -20dB when each of the other elements is active.

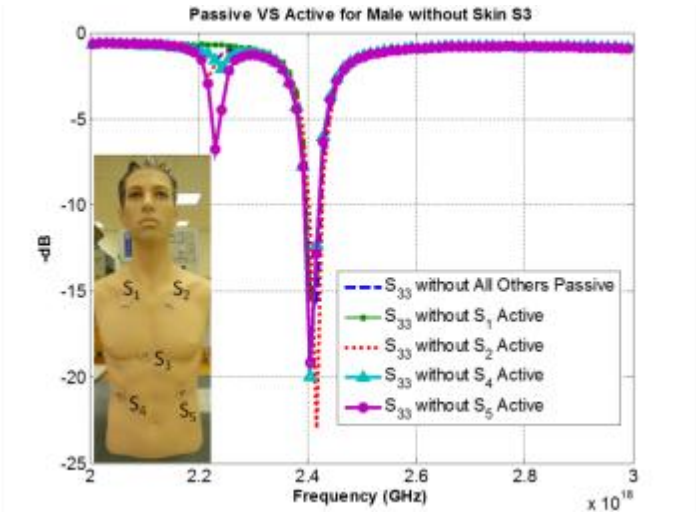

Figure 50 Passive and Active Element Return Loss for S3 on Male without Skin

In Figure 51, the return loss for Antenna S4 is -22dB within ISM band when all other elements are passive, and between -15dB and -25dB when each of the other elements is active.

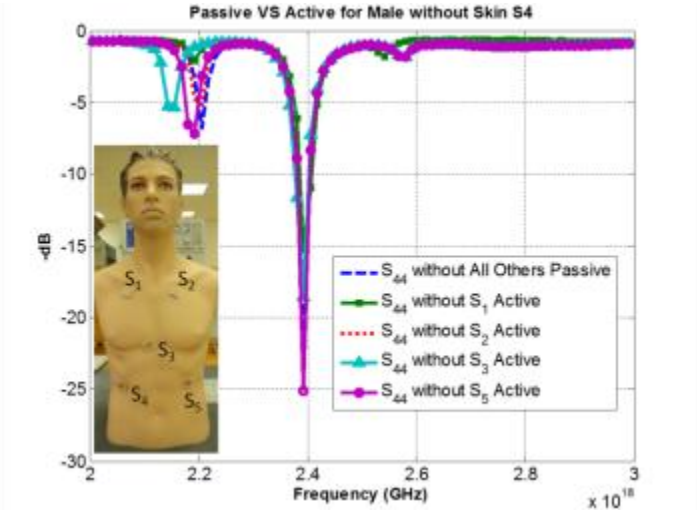

Figure 51 Passive and Active Element Return Loss for S4 on Male without Skin

In Figure 52, the return loss for Antenna S5 is -12dB within ISM band when all other elements are passive, and around -12dB when each of the other elements is active.

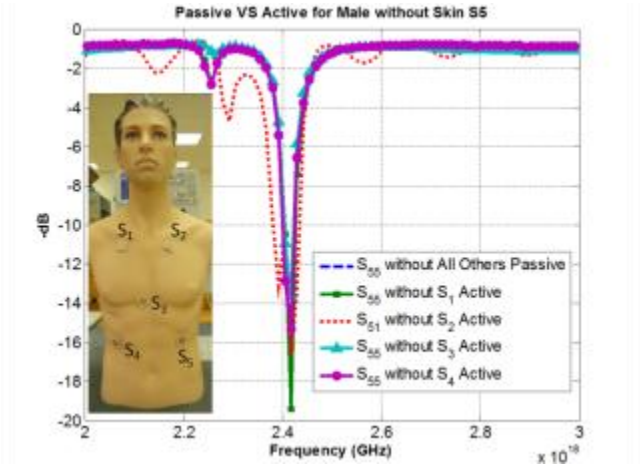

Figure 52 Passive and Active Element Return Loss for S5 on Male without Skin

Figures 53-57 show the results for the male mannequin with skin. In Figure 53, the return loss for Antenna S1 is -17dB within ISM band when all other elements are passive, and between -16dB and -18dB when each of the other antennas is active.

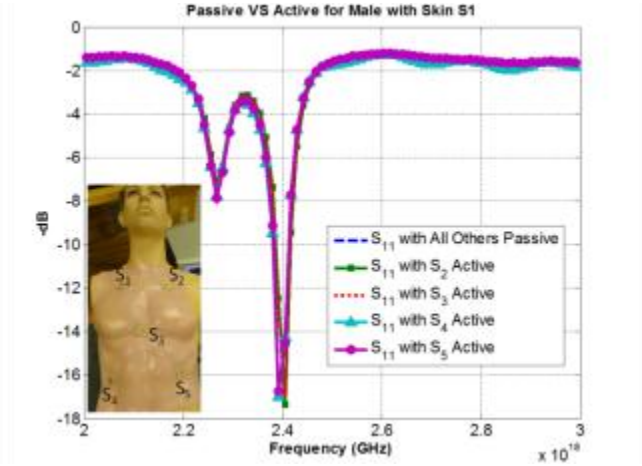

Figure 53 Passive and Active Element Return Loss for S1 on Male with Skin

In Figure 54, the return loss for Antenna S2 is -11dB within ISM band when all other elements are passive, and between -8dB and-11dB when each of the other elements is active.

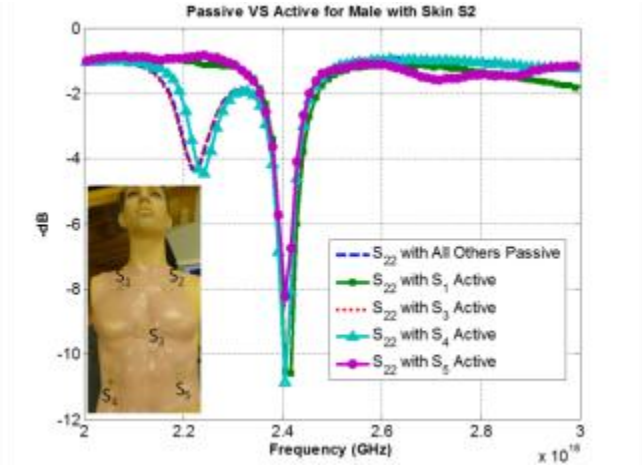

Figure 54 Passive and Active Element Return Loss for S2 on Male with Skin

In Figure 55, the return loss for Antenna S3 is -27dB within ISM band when all other elements are passive, and between -18dB and -25dB when each of the other elements is active.

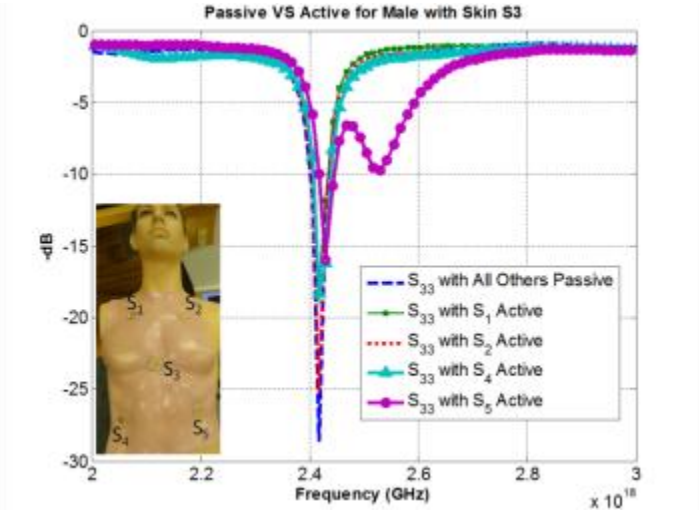

Figure 55 Passive and Active Element Return Loss for S3 on Male with Skin

In Figure 56, the return loss for Antenna S4 is -12dB within ISM band when all other elements are passive, and between -11dB and -13dB when each of the other elements is active.

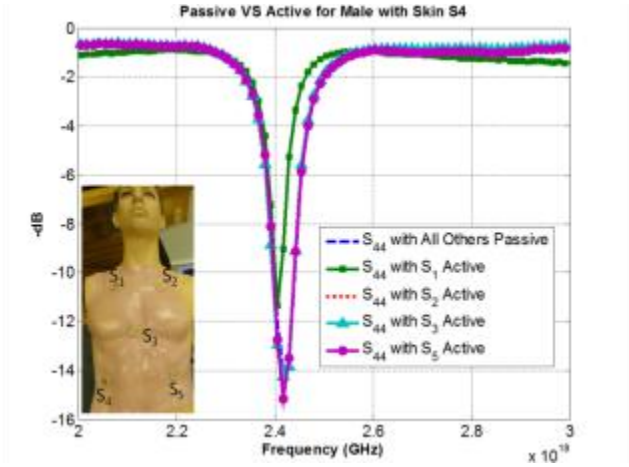

Figure 56 Passive and Active Element Return Loss for S4 on Male with Skin

In Figure 57, the return loss for Antenna S5 is -9dB within ISM band when all other elements are passive, and between -8dB and -10dB when each of the other elements is active.

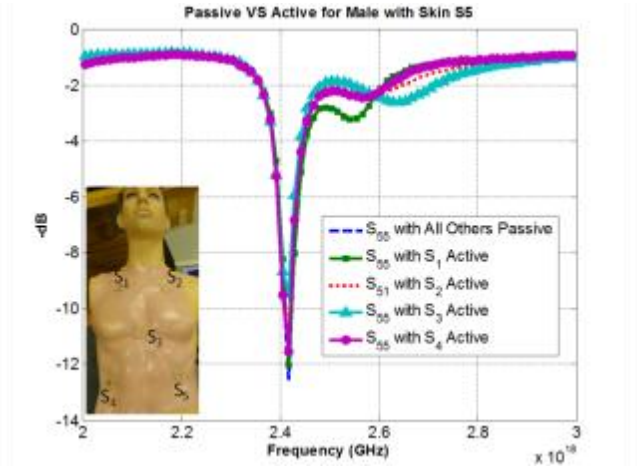

Figure 57 Passive and Active Element Return Loss for S5 on Male with Skin

Looking at the Passive and Active graphs, it can be concluded that the presence of other active antennas does slightly affect the return loss of the other antennas. However, this effect is minimal.

Female Mannequin Mutual Coupling Results

The mutual coupling between each of the antennas was also measured one pair at a time for both male and female mannequins with and without skin. Figures 58-62 show the results for the female mannequin without skin. In Figure 58, the mutual coupling between S1 and the other elements ranges from -32dB to -43dB within ISM band.

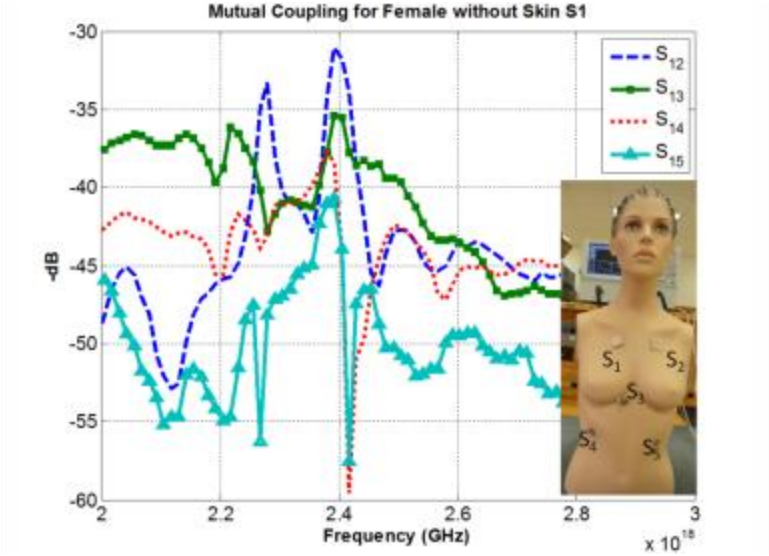

Figure 58 Mutual Coupling with S1 for Female without Skin

In Figure 59, the mutual coupling between S2 and the other elements ranges from -32dB to -44dB within ISM band.

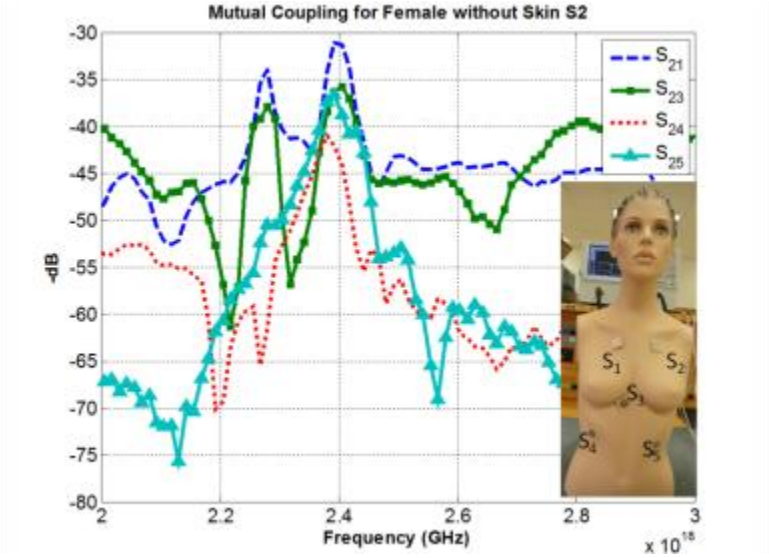

Figure 59 Mutual Coupling with S2 for Female without Skin

In Figure 60, the mutual coupling between S3 and the other elements ranges from -35dB to -42dB within ISM band.

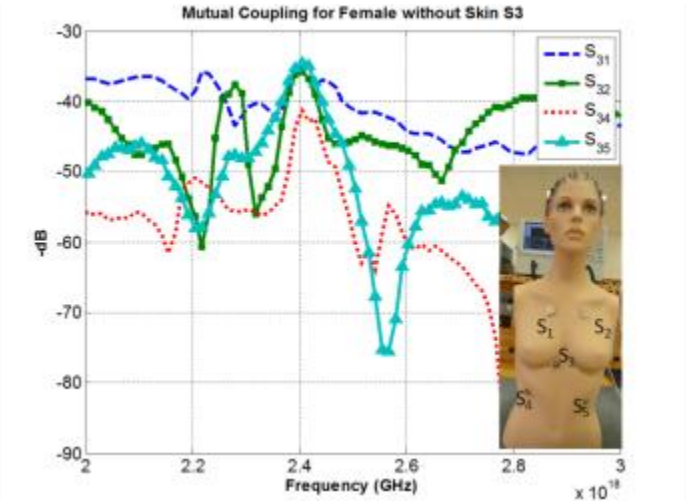

Figure 60 Mutual Coupling with S3 for Female without Skin

In Figure 61, the mutual coupling between S4 and the other elements ranges from -38dB to -45dB within ISM band.

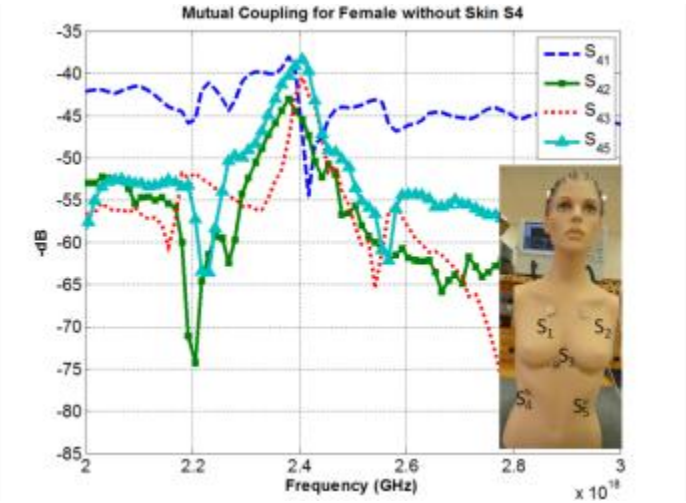

Figure 61 Mutual Coupling with S4 for Female without Skin

In Figure 62, the mutual coupling between S5 and the other elements is ranges from -35dB to -43dB within ISM band.

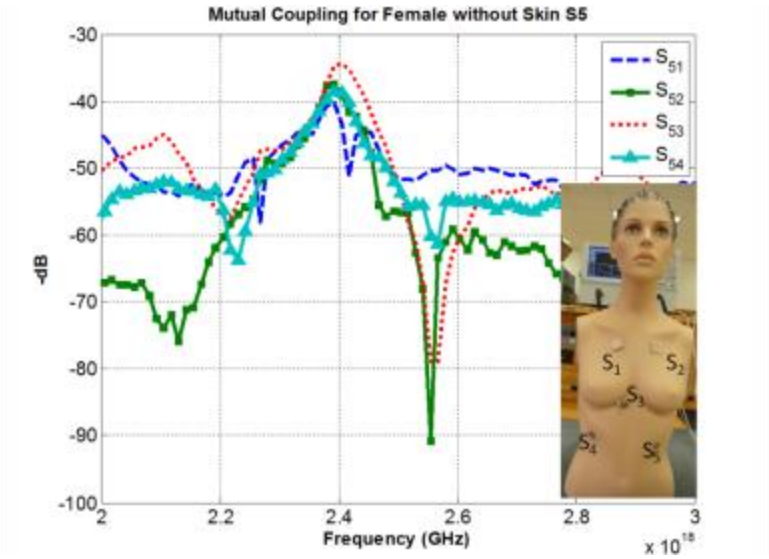

Figure 62 Mutual Coupling with S5 for Female without Skin

Figures 63-67 show the results for the female mannequin with skin. In Figure 63, the mutual coupling between S1 and the other elements ranges from -32dB to -43dB within ISM band.

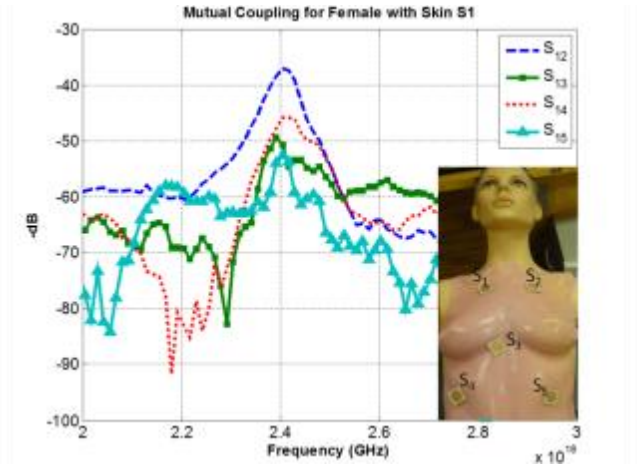

Figure 63 Mutual Coupling with S1 for Female with Skin

In Figure 64, the mutual coupling between S2 and the other elements ranges from -32dB to -44dB within ISM band.

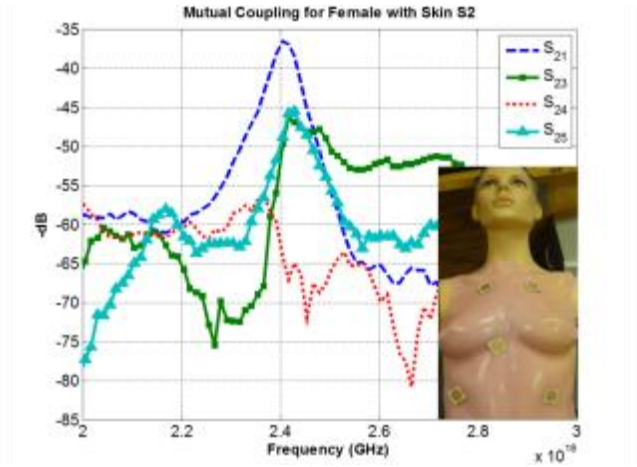

Figure 64 Mutual Coupling with S2 for Female with Skin

In Figure 65, the mutual coupling between S3 and the other elements ranges from -35dB to -42dB within ISM band.

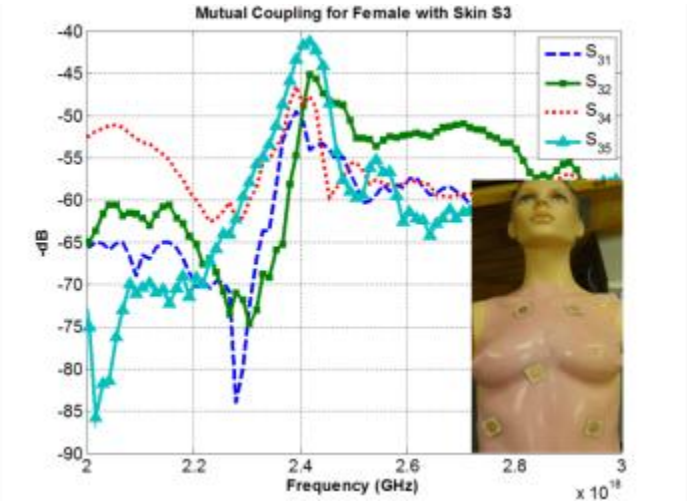

Figure 65 Mutual Coupling with S3 for Female with Skin

In Figure 66, the mutual coupling between S4 and the other elements ranges from -38dB to -45dB within ISM band.

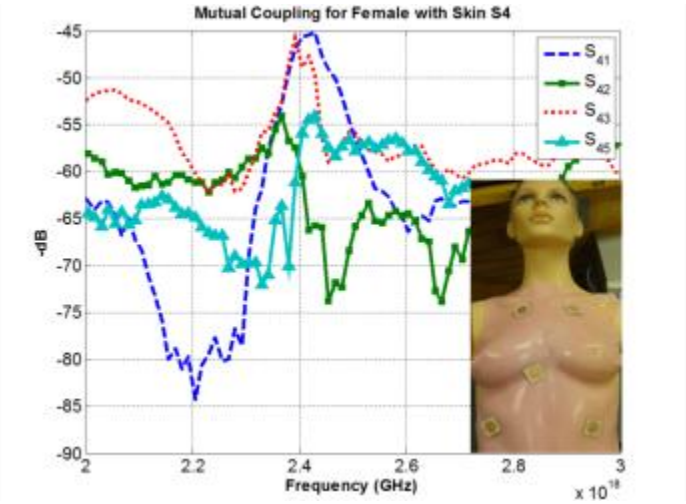

Figure 66 Mutual Coupling with S4 for Female with Skin

In Figure 67, the mutual coupling between S5 and the other elements is ranges from -35dB to -43dB within ISM band.

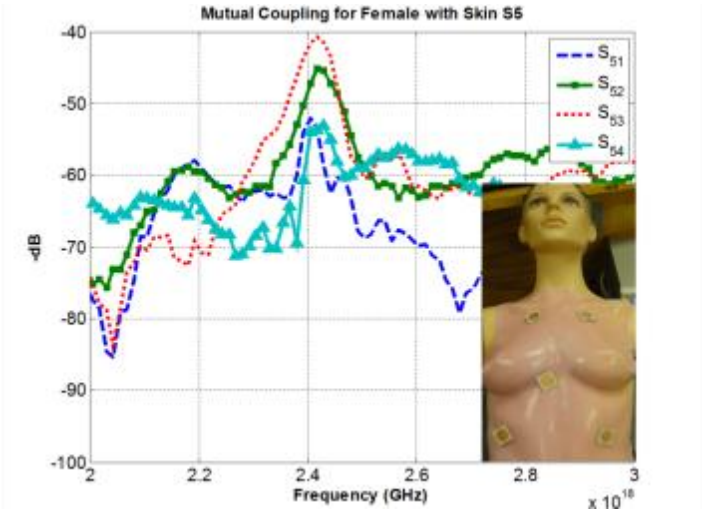

Figure 67 Mutual Coupling with S5 for Female with Skin

Male Mannequin Mutual Coupling Results

Figures 68-72 show the results for the male mannequin without skin. In Figure 68, the mutual coupling between S1 and the other elements ranges from -32dB to -43dB within ISM band.

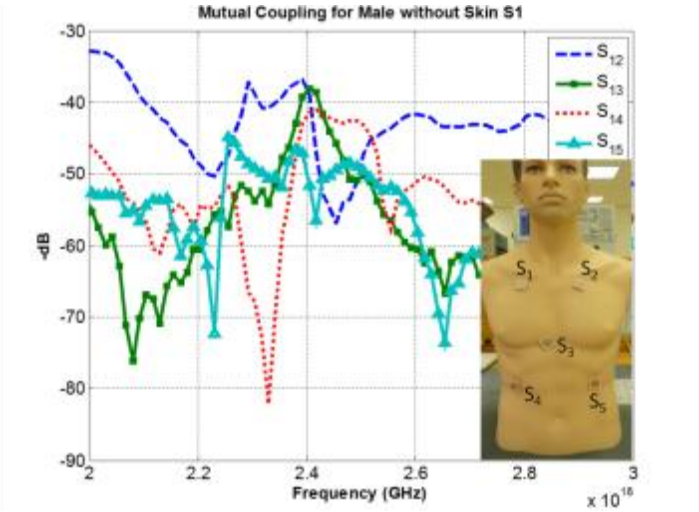

Figure 68 Mutual Coupling with S1 for Male without Skin

In Figure 69, the mutual coupling between S2 and the other elements ranges from -32dB to -44dB within ISM band.

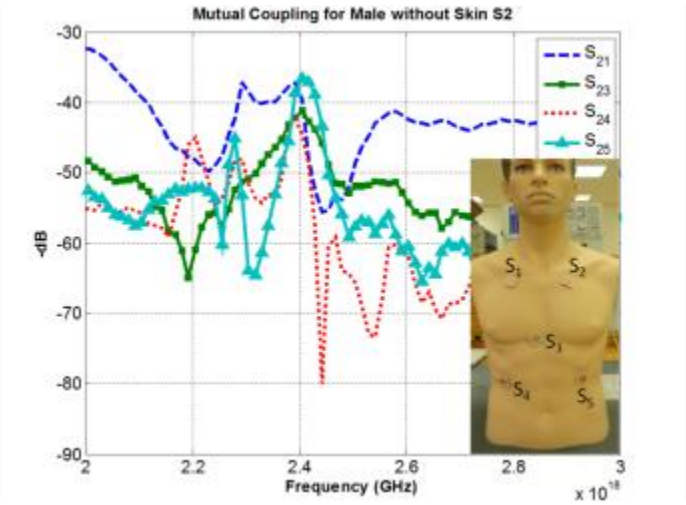

Figure 69 Mutual Coupling with S2 for Male without Skin

In Figure 70, the mutual coupling between S3 and the other elements ranges from -35dB to -42dB within ISM band.

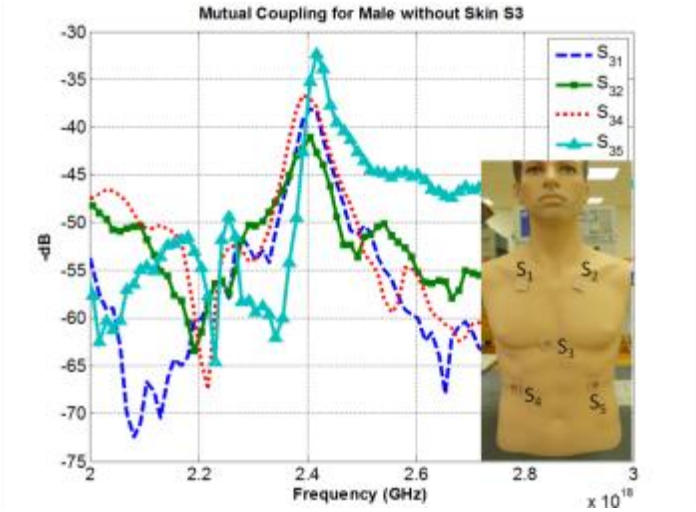

Figure 70 Mutual Coupling with S3 for Male without Skin

In Figure 71, the mutual coupling between S4 and the other elements ranges from -38dB to -45dB within ISM band.

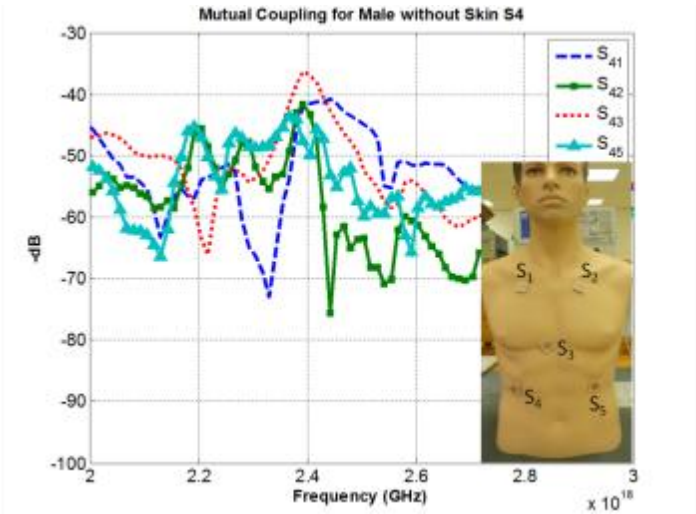

Figure 71 Mutual Coupling with S4 for Male without Skin

In Figure 72, the mutual coupling between S5 and the other elements is ranges from -35dB to -43dB within ISM band.

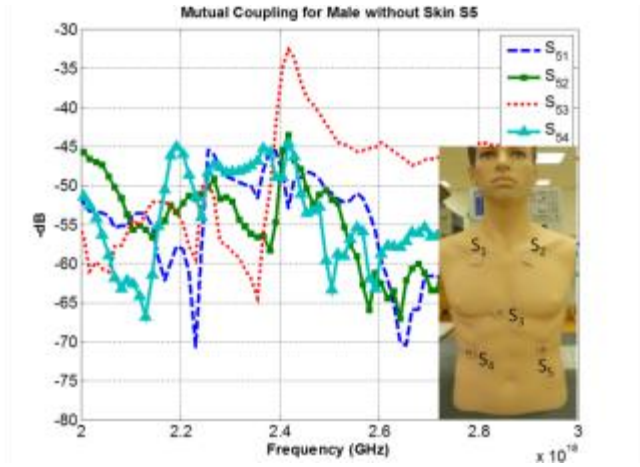

Figure 72 Mutual Coupling with S5 for Male without Skin

Figures 73-77 show the results for the male mannequin with skin. In Figure 73, the mutual coupling between S1 and the other elements ranges from -32dB to -43dB within ISM band.

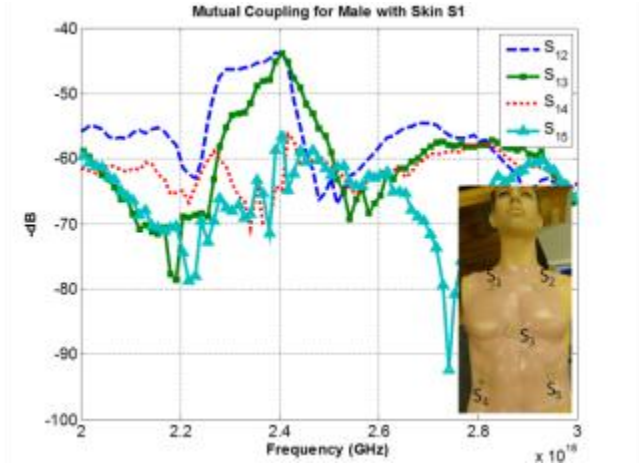

Figure 73 Mutual Coupling with S1 for Male with Skin

In Figure 74, the mutual coupling between S2 and the other elements ranges from -32dB to -44dB within ISM band.

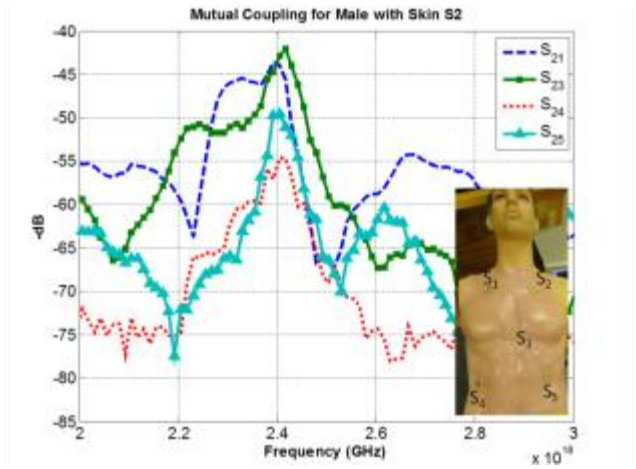

Figure 74 Mutual Coupling with S2 for Male with Skin

In Figure 75, the mutual coupling between S3 and the other elements ranges from -35dB to -42dB within ISM band.

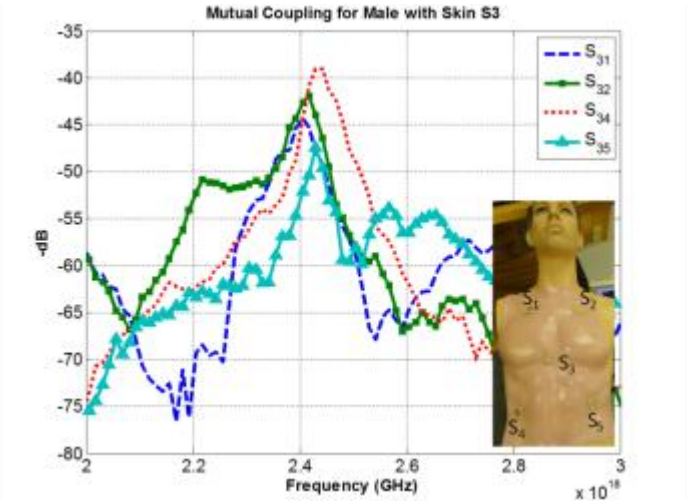

Figure 75 Mutual Coupling with S3 for Male with Skin

In Figure 76, the mutual coupling between S4 and the other elements ranges from -38dB to -45dB within ISM band.

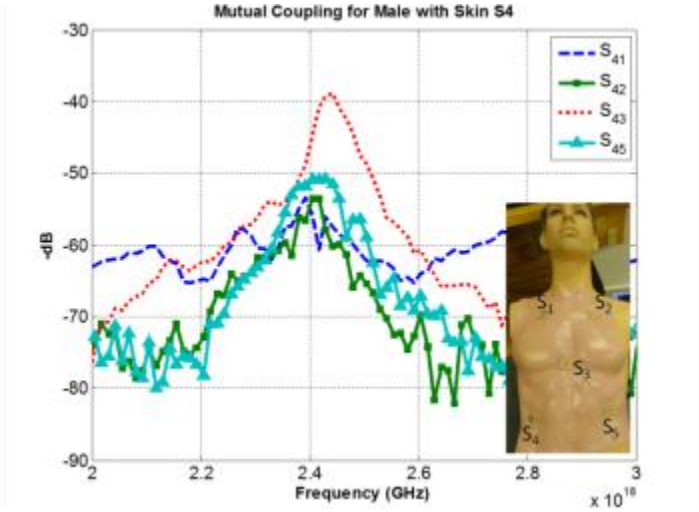

Figure 76 Mutual Coupling with S4 for Male with Skin

In Figure 77, the mutual coupling between S5 and the other elements is ranges from -35dB to -43dB within ISM band.

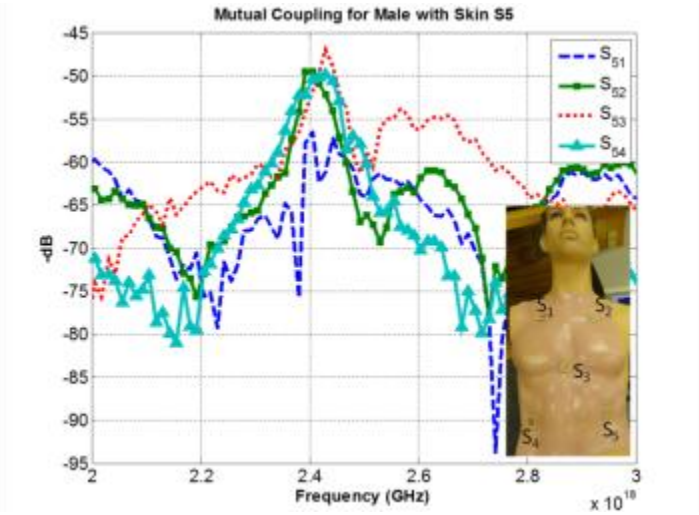

Figure 77 Mutual Coupling with S5 for Male with Skin

Mannequin Testing Mutual Coupling Comparisons

Figures 78-82 show how mutual coupling is affected with the introduction of the skin layer for both male and female mannequins. Figure 78 shows the mutual coupling on

a female mannequin between S1 and S2 with and without skin. Note that the waveforms are similar, especially from 2.35GHz to 2.45GHz, and that the presence of the skin layer lessens the mutual coupling.

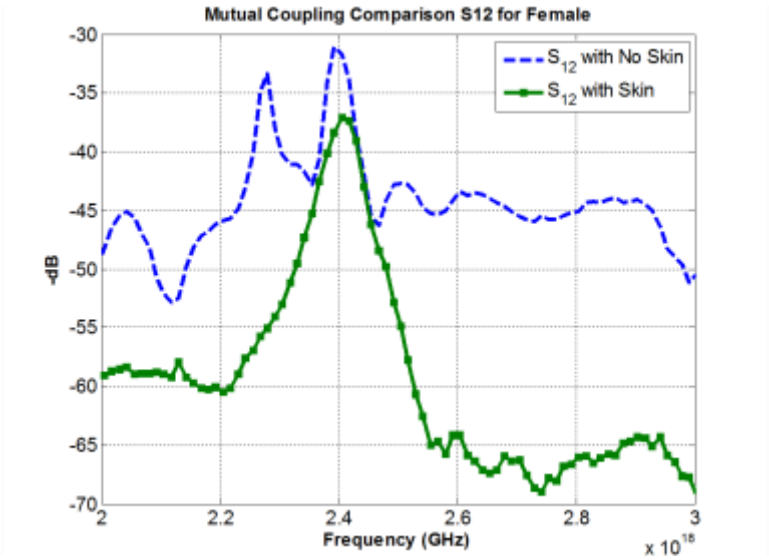

Figure 78 Mutual Coupling Skin/No Skin Comparison with S12 for Female

Figure 79 shows the mutual coupling on a female mannequin between S1 and S3 with and without skin. Like S12, the waveforms are similar with both mutual coupling peaks within ISM band and less mutual coupling with the skin layer.

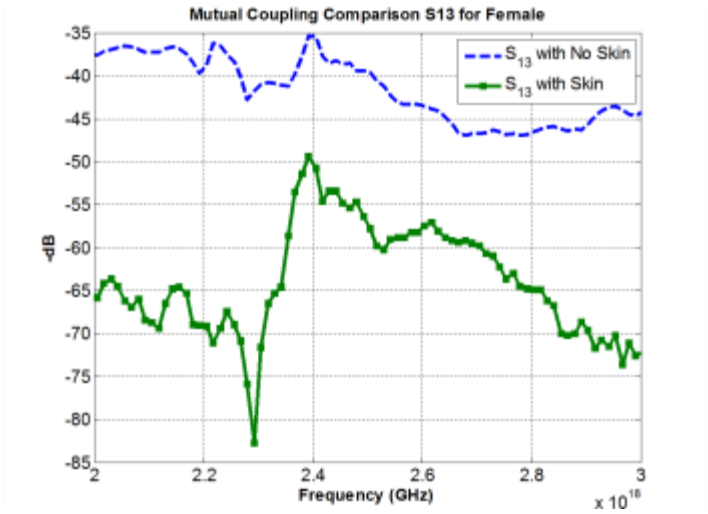

Figure 79 Mutual Coupling Skin/No Skin Comparison with S13 for Female

Figure 80 shows the mutual coupling on a female mannequin between S1 and S4 with and without skin. In this case the waveforms are not too similar. Also, unlike the previous two, mutual coupling is nearly the same within ISM band with the skin layer making only a slight difference.

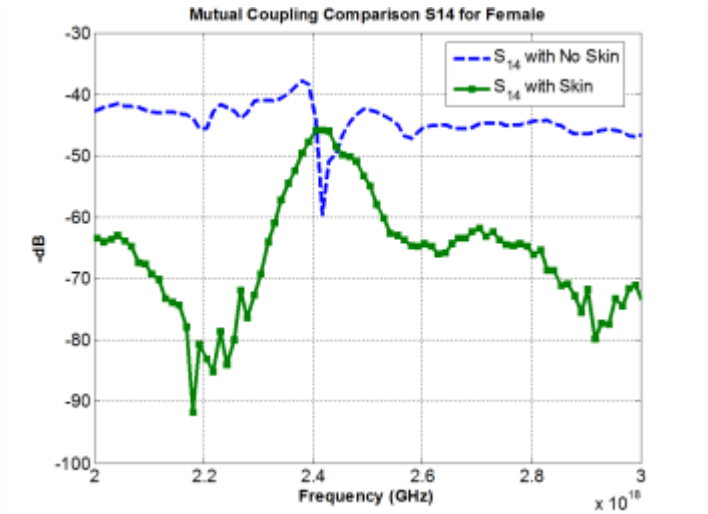

Figure 80 Mutual Coupling Skin/No Skin Comparison with S14 for Female

Figure 81 shows the mutual coupling on a female mannequin between S1 and S5 with and without skin. These two waveforms are somewhat similar and like the others, the mutual coupling is lessened by the skin layer.

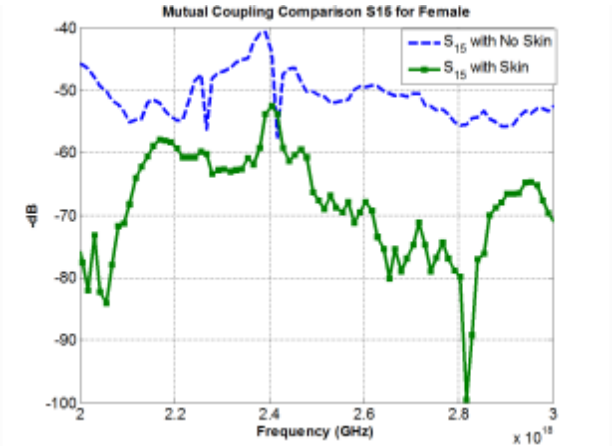

Figure 81 Mutual Coupling Skin/No Skin Comparison with S15 for Female

Figure 82 shows the mutual coupling on a male mannequin between S1 and S2 with and without skin. As expected the skin layer, reduced the mutual coupling. Also, in this case the waveforms are very similar.

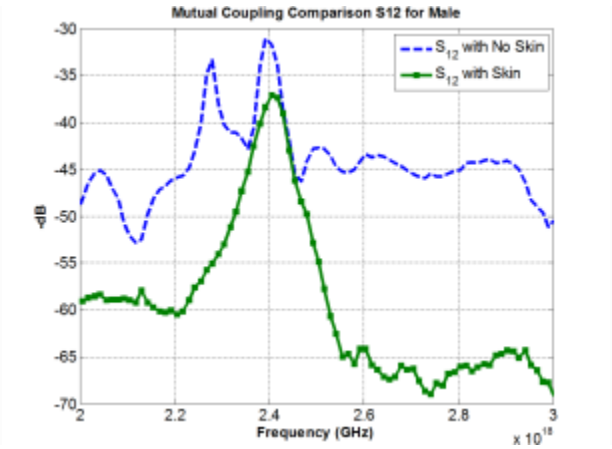

Figure 82 Mutual Coupling Skin/No Skin Comparison with S12 for Male

Figure 83 shows the mutual coupling on a male mannequin between S1 and S3 with and without skin. Like S12, the mutual coupling is reduced by the skin layer and the waveforms are very similar.

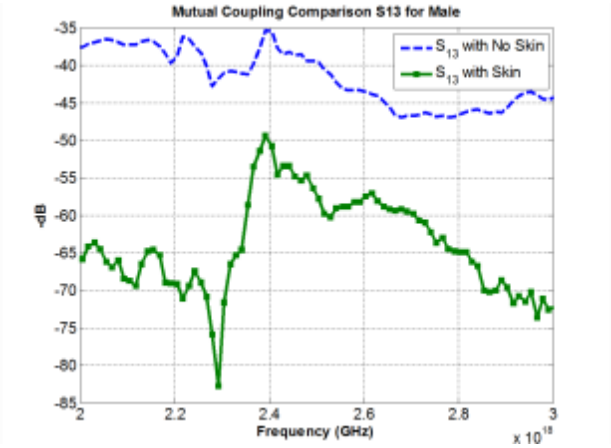

Figure 83 Mutual Coupling Skin/No Skin Comparison with S13 for Male

Figure 84 shows the mutual coupling on a male mannequin between S1 and S4 with and without skin. Unlike the previous three male examples, the waveforms for S14 are different. However, the mutual coupling with the skin layer is reduced.

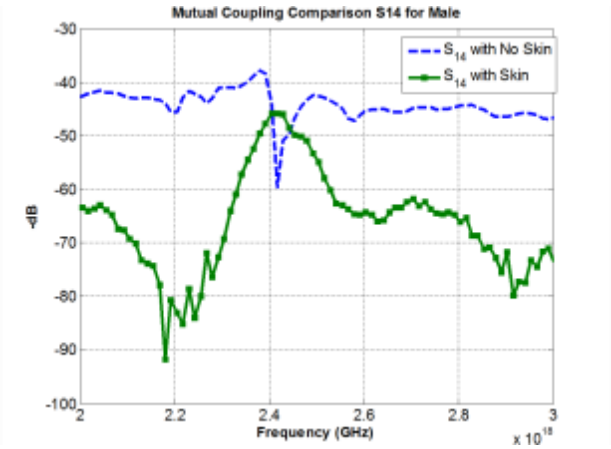

Figure 84 Mutual Coupling Skin/No Skin Comparison with S14 for Mal

Figure 85 shows the mutual coupling on a male mannequin between S1 and S5 with and without skin. As expected the mutual coupling is reduced by the skin layer.

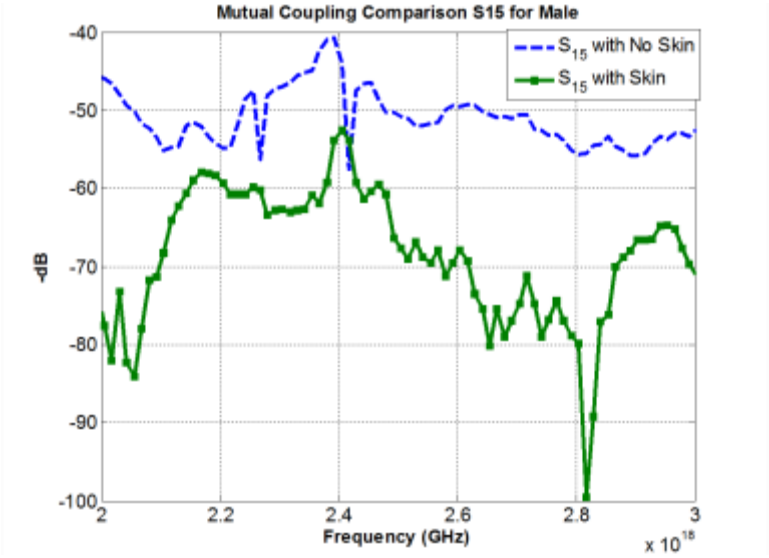

Figure 85 Mutual Coupling Skin/No Skin Comparison with S15 for Male

Torso Simulation and Mannequin Testing Comparisons

The next Figures analyze the simulated torso data compared to the testing data. Since the simulated torso was a simple model of the male mannequin, all testing results are of the male mannequin. Figure 86 shows a comparison of the mutual coupling of the simulated torso with the male mannequin without skin. For S15 and S13 the mutual coupling for the male mannequin without skin is slightly less than that of the simulated torso by 6dB's, and for S14 the mutual coupling is the same. However, for S12 the mutual coupling is slightly greater for the mannequin than it is for the simulated torso at 5dB.

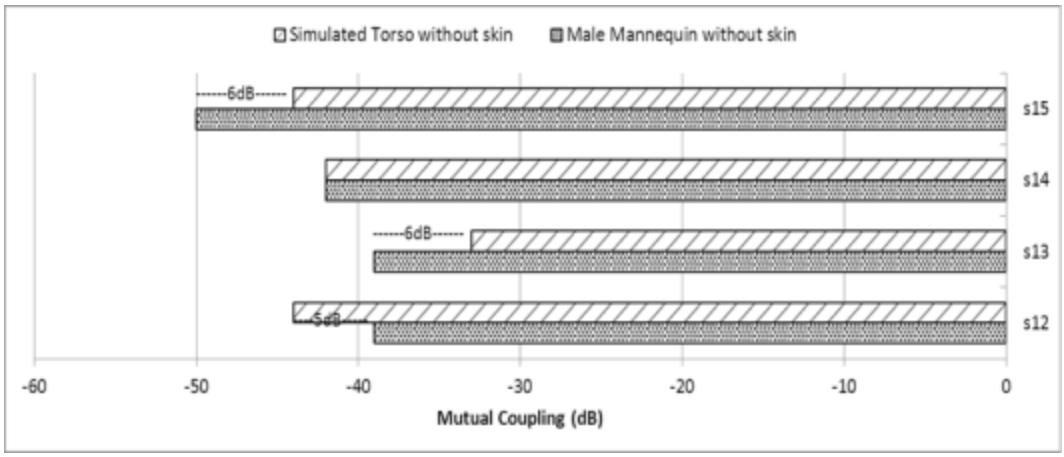

Figure 86 Mutual coupling of the simulated torso with the male mannequin without skin

Figure 87 shows a comparison of the mutual coupling of the simulated torso with the male mannequin with skin. For S12, S13, and S15 the mutual coupling for the male mannequin with skin is slightly less than that of the simulated torso by 3dB, 10dB, and 6dB, respectively. However, for S14 the mutual coupling is much less for the mannequin than it is for the simulated torso by 25dB.

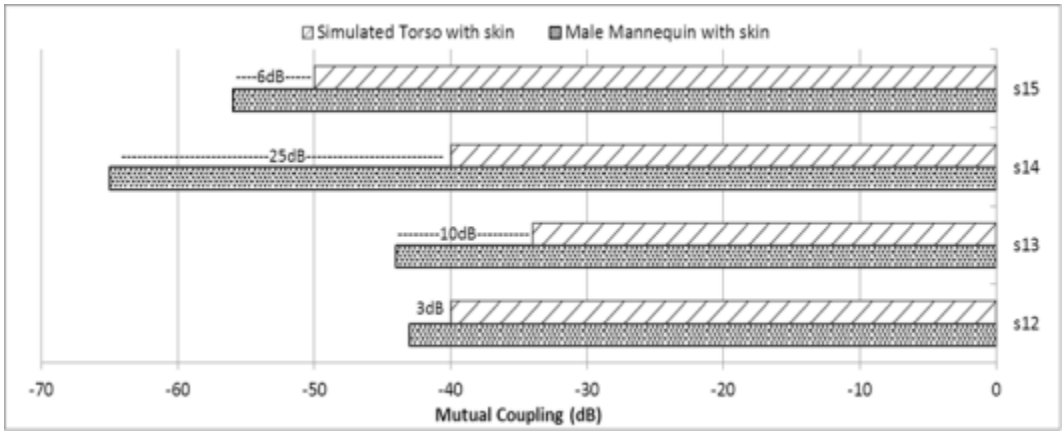

Figure 87 Mutual coupling of the simulated torso with the male mannequin with skin

CHAPTER V

CONCLUSION AND FUTURE WORK

In conclusion, a body centric antenna for wireless cardiac monitoring has been designed, simulated, and tested. The simulation and testing indicates low mutual coupling between antennas of varying distances has been achieved. In addition, the simulation and testing indicate that a thin layer of skin over the test subject further reduces mutual coupling, thus limiting interference, which is ideal.

Future work in this research is to design a complete body centric system complete with electrodes to monitor patient cardiac health. Also, different configurations other than the Holter monitor should be explored.

REFERENCES

[1] "Heart Disease Facts," 2006. http://www.cdc.gov/heartdisease/facts.htm.

[2] "Cardiac monitor," Mosby's Medical Dictionary, 8th edition. 2009. Elsevier 8 Jul. 2011 http://medical-dictionary.thefreedictionary.com/cardiac+monitor

[3] Jacobson, Carol. "Beside Cardiac Monitoring," American Association of Critical-Care Nurses. 2003; 23:71-73. http://ccn.aacnjournals.org/content/23/6/71.full.pdf.

[4] Drew, Barbara J. "Celebrating the 100th Birthday of the Electrocardiogram: Lessons Learned From Research in Cardiac Monitoring," American Journal of Critical Care. 2002; 11: 378-386. http://ajcc.aacnjournals.org/content/11/4/378.full.pdf

[5] "How EKG Machines Really Work," http://www.medicalmachinesonline.com/articles/how-ekg-machines-really-work.html

[6] "Heart CPR," 2009. http://heartcpr.com/index-4.html.

[7] Drew, Barbara J. "Cardiac Monitoring (rev)," American Association of Critical Care Nurses. 2002. http://www.aacn.org/WD/Practice/Docs/REV4_02_pocket_card.pdf

[8] "Holter Monitor," MayoClinic. 2011. http://www.mayoclinic.com/health/holter-monitor/MY00577/METHOD=print

[9] "Common Tests for Arrhythmia," American Heart Association. 2011. http://www.heart.org/HEARTORG/Conditions/Arrhythmia/SymptomsDiagnosisMonitoringofArrhythmia/Common-Tests-for-Arrhythmia_UCM_301988_Article.jsp

[10] "Holter Monitoring," 2008. http://afibtreatment.com/holter-monitoring.html

[11] Hall P. S., Hao, Y. "Antennas and Propagation for Body Centric Communications," Microwave Journal. http://www.mwjournal.com/BGDownload/bodycentric.pdf

[12] “Imagery,” Cardionet. 2007. http://www.cardionet.com/media_08.htm

[13] “Corventis Announces FDA Clearance and US Launch of the Nuvant Mobile Cardiac Telemetry System,” 2010. http://www.corventis.com/docs/NUVANT-US-Launch-FINAL.pdf

[14] Dancsisin, Mary Virginia. “Characterization of Tissue Mimicking Materials for Testing of Microwave Medical Devices,” 2011. Unpublished Master’s Thesis, Mississippi State University, Mississippi